J. Electrical Systems 20-9s (2024): 2733-2759

[1]Mr.D Venkatabrahmanaidu
[2]Dr.R.Thamizhselvan
[3]Dr.Ch. Chengaiah

Study of AI-Driven MPPT in AC/DC Microgrid with Type-III Fuzzy Controller Enhanced by Bacterial Foraging Algorithm

Abstract: - The ongoing shift towards sustainable energy solutions has driven the development of microgrids, which offer a promising approach to ensure reliable and environmentally friendly energy production. This research presents a novel microgrid design that incorporates a variety of solar energy harvesting methods, including rooftop solar panels, photovoltaic cells, floating photovoltaic arrays and grid-connected PV systems with Batteries. DC-DC converters are used as power converters between load and source in order to amplify or increase the PV power depending on the output voltage. This study helps to provide a robust energy solution that not only meets fluctuating load requirements, but also strengthens the energy system against the disturbances associated with solar energy. This design incorporates an intelligent control system controlled by an Interval Type-3 fuzzy logic controller. The controller is meticulously designed to deal with the uncertainties and non-linear characteristics of renewable energy systems and to ensure optimal performance under varying weather and load profiles. The analysis in this microgrid uses an artificial intelligence-driven Maximum Power Point Tracking system that dynamically adjusts the operating parameters to utilize the maximum energy yield from the solar systems. A further improvement in the control strategy is achieved through the use of a bacterial foraging optimization algorithm. This advanced algorithm fine-tunes the fuzzy controller parameters, significantly increasing the efficiency and stability of the microgrid's power generation. The synergy between the Interval Type-3 fuzzy logic controller and the BFOA results in a resilient and adaptive control system that can efficiently deliver high quality energy. Extensive simulations were conducted using MATLAB Simulink 2023b to validate the performance of the proposed microgrid design and control architecture. The empirical results show that the integrated system effectively optimizes the energy flow of different solar systems, maintains power stability and achieves superior efficiency. The study pushes the boundaries of microgrid design and provides a scalable and smart energy solution that paves the way for the widespread adoption of renewable microgrids in different geographical areas.

Keywords: Artificial Intelligence(AI), Bacterial Foraging Optimization Algorithm (BFOA) Interlinking Converter, Interval Type-3 Fuzzy Controller, Microgrid, Maximum Power Point Tracking system(MPPT), Boost Converter and STATCOM.

1. Introduction

In the face of global warming, it is imperative to prioritize the reduction of carbon emissions and the transition to renewable energy sources in the energy sector. This is crucial for the sustainability of our planet and the well-being of future generations. a group of interconnected loads and decentralized energy resources that acts as a single controllable entity in relation to the grid. i.e. microgrids (MG). It plays a critical role in integrating distributed renewable energy generation such as photovoltaic (PV), wind power with energy storage systems, combined heat and power (CHP) systems, fuel cells and electric vehicles (EVs) into the grid. By operating as self-sufficient systems, MGs can continue to provide power to critical loads during grid outages or emergencies, reducing the impact of power outages on communities, businesses and essential services. The challenges posed by the unpredictable nature of renewable energy sources, which are dependent on fluctuating weather conditions and whose energy production is not entirely predictable, are usually overcome by using multiple energy sources. To overcome the above challenges and improve energy efficiency, controllers are equipped as an integral part of any microgrid operation and serve as the brain for managing various energy sources, storage systems and loads. These devices continuously monitor grid conditions and adjust parameters such as current flow, voltage and frequency to ensure grid stability and reliability [1,2,3,4].

[1] Research Scholar, Department of Electrical Engineering, Annamalai University, Annamalainagar, Tamil Nadu, India, Email: dvb.naidupeed@gmail.com
[2] Associate Professor, Annamalai University, Department of Electrical Engineering, Chidambaram, Tamil Nadu, India, Email: tamil2012au@gmail.com
[3] Professor, Department of Electrical Engineering, S.V.U College of Engineering, Sri Venkateswara University Tirupati, India, Email: chinthapudisvu@gmail.com
* Corresponding author E-mail: dvb.naidupeed@gmail.com

At the beginning of this section, a detailed introduction to the MPPT algorithms for solar systems with artificial intelligence is required. The active power (P) of a solar power system with PV panels is affected by solar irradiance (E) and operating temperature (T), especially under rapidly changing partial shading conditions due to the nonlinear nature of photovoltaic cells. The complicated correlation between power output and PV input parameters leads to suboptimal power extraction, prompting researchers to focus on AI-based MPPT methods as an alternative to traditional perturbation and observation techniques to maximize the performance of wind turbines and PV systems. Several applications have been used in grids as a result of the introduction of new technologies in the development of controllers and converters [5]. These include solar arrays, fuel cells, wind turbines, small diesel generators, small hydroelectric plants, backup energy systems, and DC/AC load systems for energy demand. It is difficult to develop a hybrid system with all renewable and non-renewable energy sources, storage devices, converters and loads. In most hybrid systems, the DC components are the wind turbine, the solar panels and the battery bank, while the AC components are the diesel generator and the load. The conversion from AC to DC and vice versa is performed by an IGBT-based high-power converter [6]. Constant power loads (CPLs) in DC-MGs reduce the effective damping of the DC-DC converter and can have destabilizing effects since CPLs have nonlinear dynamics and negative incremental impedance [7-8]. An MG can be either a DC network or a mixture of DC and AC. Therefore, a DC microgrid is the best option for operating renewables, power converters and modern loads, all of which require DC power. Several non-linear control methods are used for a regulated DC bus voltage and stable operation.

In the past, linear PI/PID control, SMC and AI-based control have been used in some cases to control MG. However, in the last decade, much attention has been paid to the intelligent control of nonlinear systems [9]. As a result, common controls such as neural networks, fuzzy and neuro-fuzzy controls have been explored. in 1965, Zadeh introduced fuzzy logic for use in cellular robotics. Since then, numerous studies have applied this fuzzy logic to various modelling in control systems. It provides a framework for understanding the uncertainties and opacity of the entire model through human reasoning based on membership functions and linguistic variables. The application of fuzzy logic controllers (FLC) to the operation and control of power grids has become increasingly important in recent years [10]. Fuzzy controllers are excellent at dealing with non- linearities and uncertainties associated with renewable energy sources and loads, and provide superior performance in scenarios where conventional controllers struggle to maintain stability. The Integral Fuzzy Type-3 controller used in this research offers several advantages for microgrid control. By integrating fuzzy logic with proportional-integral-derivative control, this controller combines the adaptability and robustness of fuzzy logic with the ability of integral behavior to eliminate steady-state errors.

Bacterial foraging optimization, also known as BFOA, is a bio-inspired metaheuristic algorithm based on the foraging behaviour of Escherichia coli bacteria. It is used to solve optimization problems by gradually refining a population of potential solutions towards an optimal solution. The main goal of this process is to improve the controller's performance in terms of precision, resilience and effectiveness by iteratively adjusting the fuzzy logic membership functions and other parameters using the BFOA. This allows the controller to adapt and improve its performance even in difficult and unpredictable environments [11,12,13].

Another crucial component in most MG’s are power converters, which help to connect the AC and DC grids in addition to maintain the stability of the entire microgrid. A bi-directional droop control approach has been utilised along with Bi-directional DC/AC converters to measure the power demand of the AC and DC miFcrogrids depending on the frequency of the AC terminal bus and the voltage of the DC terminal bus, respectively. Moreover, the amplitude and direction of the power transfer through the power converters are deter- mined [14]. To maintain a constant DC link voltage, primary or local control with PV cells and batteries is used. To provide a stable voltage, ensure smooth grid synchronization and ensure proper sharing of active power between the DC and AC buses, the secondary or system level is achieved by controlling the intercom nested converter located between the AC and DC buses.

In a hybrid microgrid, the interconnected converter (ILC) plays a crucial role in connecting the AC and DC grids. Its control strategy has an impact on energy flow management, power quality, system efficiency and stability. The ILC is normally controlled as a current source, resulting in poor dynamic stability when a remote, weak AC sub-grid with a high connection impedance is connected. In times of surplus energy generation, e.g. during strong weather, the storage devices are used in microgrids to temporarily store this surplus energy for later use. Likewise the energy generation is not sufficient to cover the increasing load demand then the stored energy is utilized [15,16].

To link the sections presented above and ensure proper energy transaction, Artificial Intelligence (AI) is revolutionizing the operation and control of microgrids by providing advanced algorithms to optimize energy generation, storage and consumption. Through machine learning and predictive analytics, AI can forecast renewable energy generation, predict fluctuations in demand and dynamically adjust microgrid parameters in real time. This enables microgrids to achieve higher efficiency, reliability and resilience while seamlessly integrating different energy sources. The study on AI-driven Maximum Power Point Tracking (MPPT) in AC/DC microgrids with an interval type III fuzzy controller enhanced by the Bacterial Foraging Algorithm (BFA) presents a sophisticated approach to optimize the performance of renewable energy systems. In the following sections, Work Motivation, detailed view of MG Components, mathematical modelling of the relevant components in MG and the simulated experimental results of this research work and other requirements are described in detail.

2. Literature review

Prepare Hybrid power supply systems based on renewable energies are increasingly being used worldwide to reduce carbon emissions. However, renewables are sporadic and incredibly unpredictable, which can lead to significant frequency fluctuations. By using optimally designed control systems, these fluctuations can be kept within the appropriate limits. Maximum Power Point Tracking (MPPT) becomes the focus of study to increase the efficiency of the solar system and ensure that the operating point is always at the Maximum Power Point (MPP) to overcome the aforementioned limitations [5]. It is possible to achieve uniform peaks without abrupt irradiation or under PSC by using traditional hill-climbing (HC) MPPT approaches such as Incremental Conductance (IC) and Perturb and Observe (P&O) [6]. Despite some advantages of existing MPPT methods, AI-based MPPT methods for DC-DC converters are implemented in solar energy systems to increase the efficiency of solar energy. Electronically implemented MPPTs also include adjusting the tilt angle of solar panels to track the direction of the sun and integrating soft computing weather forecasts [7].In this research work, this AI driven MPPT trend has been successfully implemented.

Kinetic Gas Molecule Optimization (KGMO) is a state-of-the-art algorithm that uses the principles of kinetic gas molecules to optimize photovoltaic systems and increase their performance. The KGMO algorithm uses the principles of kinetic gas molecules to optimize the performance and maximize the power output of photo- voltaic systems together with ANN, which provides better results than the results of conventional MPPT schemes[29,30]. An LFC structure based on a Tilt-Fraction-Order-Integral (TI) controller and an FO-PID controller with a filter was proposed by Ahmed et al [16]. The Artificial Gorilla Troops Optimizer is used to optimally design this proposed controller. The effects of high renewable energy share on the considered power system is also investigated with the proposed controller. In [17], the performance of the system is improved with the recently developed ISSA (Improved Squirrel Search Algorithm) algorithm, which is used to adjust the parameters of several controllers, including PID, two- and three-degree PIDs, and cascaded 2DOF fractional-order PIDs (FOI). The performance of the optimal controller was modified using the integrated Particle Swarm Optimization (PSO) and Squirrel Search Algorithm (SSA). Numerous case studies have been con- ducted to evaluate the reliability, adaptability and flexibility of the system.

In [18], a hybrid energy system including a thermal system, wind and solar energy, diesel generators, electric vehicles, and energy storage systems such as batteries and superconducting magnetic energy storage is used. The frequency was controlled by a reliable FOPI frequency controller. In addition, the Water Cycle Optimization Algorithm (WOA) optimizes the FOPI parameters. The selected objective function is the Integral Time Absolute Error (ITAE). The results of the proposed algorithm are compared with those of PSO, another well-known optimization technique, to demonstrate its effectiveness. By maintaining a faster settling time, the pro- posed optimization method performs better than PSO. To address the frequency anomaly caused by the presence of renewable generation units in [19]. Microgrids are becoming increasingly popular to manage energy demand in localized areas [26]. The integration of the bacterial foraging algorithm with a fuzzy controller in microgrids offers a promising solution to optimize energy management and improve grid stability [27]. By using the bacterial foraging algorithm in conjunction with a fuzzy controller, microgrids can effectively balance energy supply and demand, thus improving the overall efficiency and stability of the grid [28].

An FLC-based EMS with AC/DC microgrid is implemented. The power quality of the MG is increased in addition to the EMS design. It proposes to analyse and manage storage devices. The FLC extends battery life and creates an ideal SoC. To reduce power quality issues caused by non-linear, unbalanced load conditions, a grid-integrated MG based on FLC is implemented. For automatic load frequency management (ALFC) of a hybrid power system, a hybrid sperm swarm optimized-gravitational search algorithm based on chaotic search is presented in [21]. The integral-time absolute error of the hybrid system is minimized to determine the control parameters of the PID controller for the ALFC, which controls the frequency of the system. The effectiveness of the proposed technique is tested with different combinations of power sources connected to the system. In addition, a sensitivity analysis is performed to investigate the flexibility of the proposed technique considering the real-time weather-related interruptions and load changes of the renewable energy sources. In [22], the innovative fuzzy PID+PID hybrid controller used for frequency regulation in a hybrid power system is optimized using the whale optimization algorithm (WOA). The proposed application of WOA approach for frequency regulation in HPS can be considered unique at this stage. Compared to other controllers, the proposed WOA-optimized fuzzy PID + PID hybrid controller performs the best, which proves the effectiveness of WOA in load frequency control experiments. Due to the spatial and temporal variability associated with renewable energy sources and the large operational uncertainties caused by the changing natural environment, the long- term optimal operation of RES is a difficult challenge. Stochastic model predictive control (MPC) based on probabilistic forecasting and rolling stochastic optimization is designed and implemented for the long-term operation of renewable energy [24].

PV energy generation systems are ranked as a top energy system by utilities around the world because they generate electricity from renewable sources. These energy options have the disadvantage of being unpredictable and dependent on climate and weather conditions. To achieve noise-free voltage reduction for DFIG and PV systems, an effective strategy using a Landsman converter has been developed [25]. The tracking point of maximum power is controlled with a PWM-based PI controller using the firefly method. A grid-synchronized 3-phase VSI with an LC filter converts the DC voltage into AC voltage, ensuring smooth operation and elimination of harmonics. The outputs have a minimum THD value.

3. Research Motivation

In today's world, there is a growing emphasis on generating electricity from sustainable sources to mitigate the impact on the environment. Researchers and energy stakeholders are exploring advanced technologies like AI, machine learning, deep learning, and fuzzy logic for developing microgrids. However, renewable energy sources such as solar radiation and wind speed are constrained by fluctuations that affect efficiency. In order to accommodate that Artificial intelligence techniques and fuzzy logic concepts are being explored to improve Power Quality in a cost-effective manner without significantly increasing costs through additional components such as converters and filters.

In this work, a study on the design of a proposed two-level control framework for stable and voltage-tracking operation of the HMG under variable generation and load changes is presented. In this paper the following considerations are necessary for design and reliable HMG operation. Firstly: Maintaining a stable DC link voltage in the variation of temperature and irradiation fluctuations through AI based MPPT. at next, this model ensure that the inverter can be precisely controlled in conjunction with the load grid and to minimize the voltage deviation from the reference voltage specified by the load. In addition, a robust control method must be implemented in the inverter in conjunction with the load grid to achieve high performance due to changes in load dynamics. Finally, it is mandate that will ensure synchronized operation between the AC and DC sides of the HMGs to enable appropriate power sharing between the primary grid and the DC side. In particular, the controller's design process has been split into two stages: one addressing stability issues through partial feed- back linearization method while another deals with robust control methods alongside operational synchronization between AC and DC sides of HMGs accomplished using VSC controlled by PI controller. This section provides an overview of the motivations behind the study, which will be further explained in succeeding sections.

4. Proposed Research Methodology

The block diagram represents an advanced hybrid AC/DC microgrid system integrating solar PV energy sources. A key feature of this system is the AI-driven Maximum Power Point Tracking (MPPT) scheme used for the

solar PV systems. In order to explore advanced control strategies, an interval type 3 fuzzy-based controller enhanced by the Bacterial Foraging Optimization Algorithm (BFOA) and interlinking drop control, ensure power quality. Here's a detailed breakdown of the elements and processes involved.

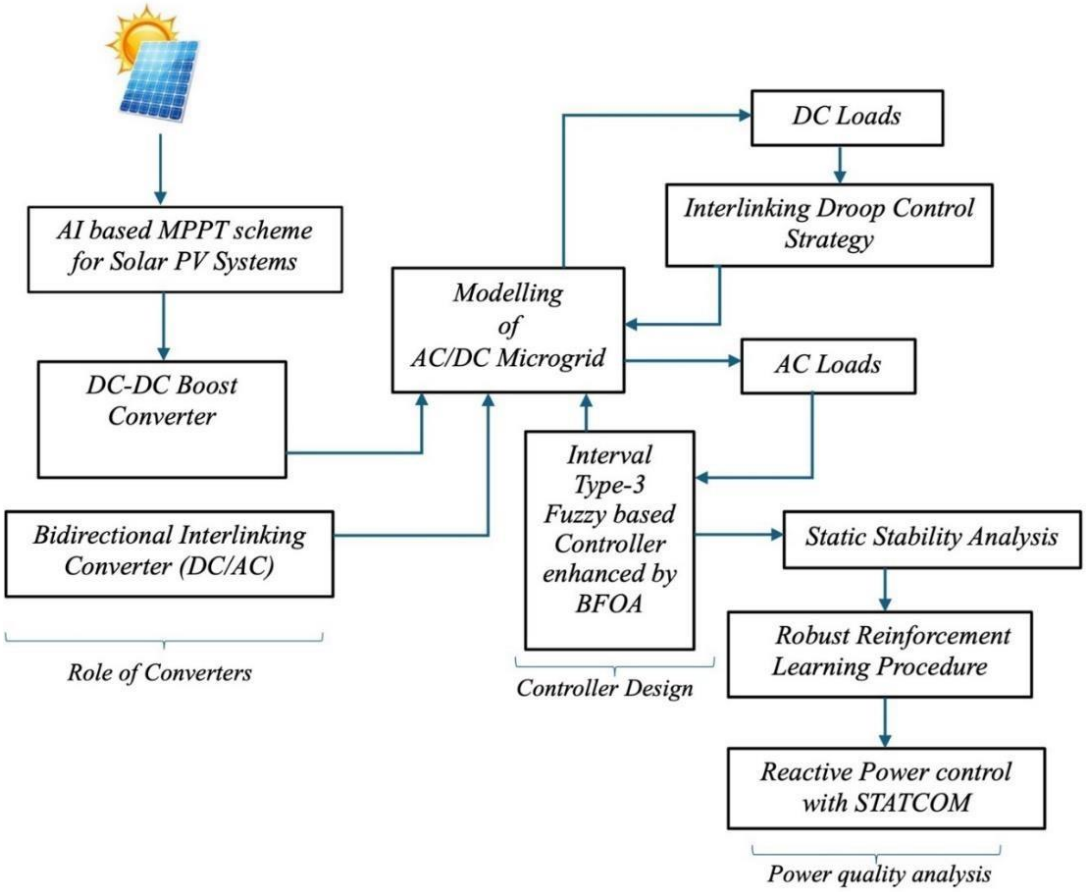

Fig.1. Block diagram for AI driven Hybrid AC/DC Microgrid

4.1 Modeling of AC/DC Microgrid

Comprehensive and accurate modelling enable researchers and industry professionals to gain valuable insights into the behaviour, performance, and control of AC/DC microgrids. The microgrid integrates both AC and DC loads, requiring thorough modelling for efficient operation and control. The dynamics of the power grid are significantly influenced by the growing adoption of renewable energy sources such as rooftop solar cells, photovoltaic, floating PV, solar PV, battery storage along with the grid (refer to Fig. 1). This system features AI-based Maximum Power Point Tracking which optimizes the power output of solar modules. A boost DC-DC converter with multiple inputs manages this optimized DC current in addition to a bi-directional link converter that facilitates current flow between AC and DC loads. Advanced control strategies including an Interval Type 3 fuzzy-based controller also improved by Bacterial Foraging Optimization Algorithm together with interlinking drop control ensure stability and quality in powering on demand needs. This proposed system delivers electricity to consumers via power converters, ensuring stable high-quality power supply even under extreme conditions. The paper discusses the use of reinforcement learning algorithms and static synchronous compensators for improving the performance and control of hybrid microgrids (Cheng et al., 2021). The paper highlights the importance of comprehensive modelling techniques and proposes an enhanced fuzzy-based en- ergy management strategy for a hybrid power system. This strategy aims to optimize power output, ensure stable high-quality power supply, and effectively manage the dynamics of the power grid.

4.2 AI-Driven MPPT Scheme for Solar PV Systems

In general, AI-based MPPT algorithms often use machine learning models such as neural networks, support vector machines, or fuzzy logic systems. These models are trained using historical data on solar irradiance and temperature, allowing them to accurately predict the maximum power point in real-time for photovoltaic systems. The use of ANN for MPPT allows for the identification and utilization of nonlinear correlations between variables in PV systems, resulting in a reliable, quick, and efficient maximum power point tracking process (Chen & Wang, 2019). Additionally, the ANN-based MPPT method eliminates the need for additional hardware and reduces dependence on system parameter variations.

This approach proves to be robust and versatile, making it a preferred choice for achieving optimal power generation in PV systems, particularly under partially shaded conditions. Furthermore, the combination of an artificial neural network controller with a scanning algorithm in this novel method enhances the tracking of the global maximum power point under partially shaded conditions, leading to improved performance and efficiency in PV systems. The proposed method, known as the ANN-KGMO MPPT controller, utilizes the Kinetic Gas Molecular Optimization Algorithm to train the developed Artificial Neural Network. This process enables the evolution of connection weights and biases to achieve optimal values for adjusting the duty cycle of the converter in accordance with PV array's Maximum Power Point, as depicted in a block diagram (refer to Fig. 2).

Real-world optimization problems are increasingly being solved by swarm-based algorithms. The optimization algorithm Kinetic Gas Molecule Optimization (KGMO), which is based on the kinetic energy of gas molecules, is presented in this study. The kinetic theory of gases, which establishes the guidelines for gas molecule inter- actions in the model, applies to the agents, which are gas molecules that are moving in the search space.

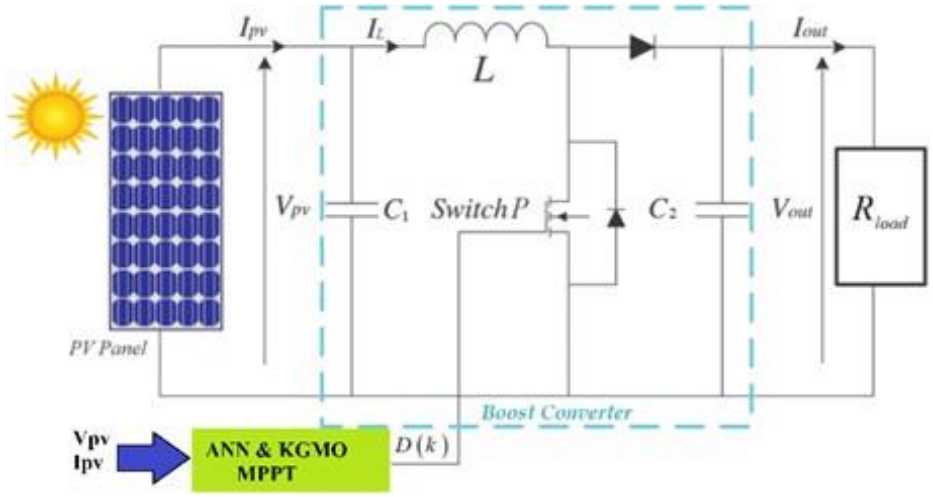

Fig. 2. Block diagram of the proposed ANN-KGMO MPPT model

The proposed MPPT algorithm involves three steps at most important i.e. data preparation and ANN training, Kinetic Gas Molecular Optimization, and applying KGMO optimized parameters to the ANN model. This approach combines data preparation and training of an Artificial Neural Network with the use of Kinetic Gas Molecular Optimization to optimize the model's parameters.

By utilizing this three-step approach, the proposed MPPT algorithm aims to effectively and accurately track the maximum power point of the photovoltaic system as depicted in Fig. 3. In this manuscript, we propose a metaheuristic optimized multilayer feed-forward artificial neural net- work controller to extract the maximum power from available solar energy. To improve the maximum power point delivered by PV arrays and overcome drawbacks in conventional MPPT methods under irradiation variation, a hybrid MPPT controller is designed. It takes PV array voltage and current as input parameters, and outputs the duty cycle of the DC/DC boost converter con- trolling power transfer between the PV array and the load. Discussion in this section will provide a summary of the Artificial Neural

Network based KGMO MPPT technique, highlighting its features and updates in managing DC power conversion for grid integration that will explained in subsequent sections.

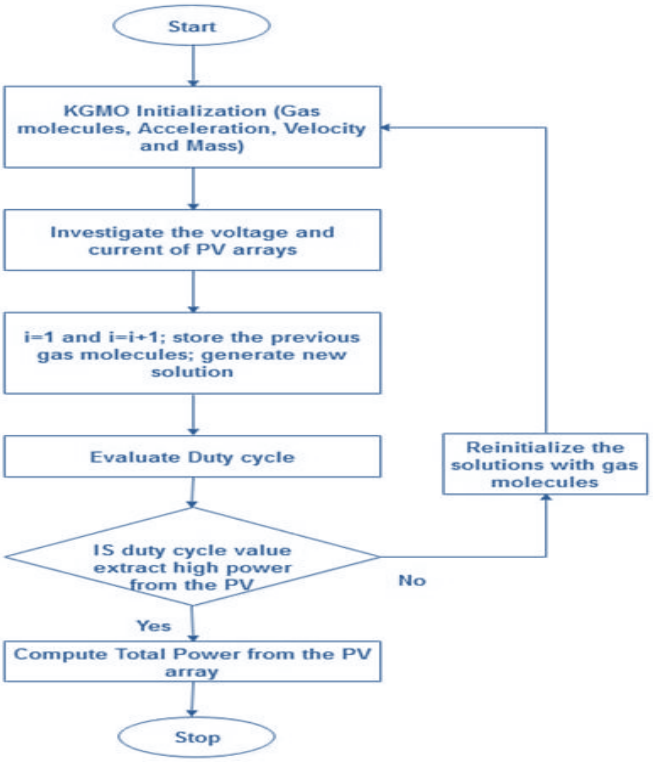

Fig. 3. Flow chart of the proposed ANN-KGMO MPPT model

4.3 Implementation of Converters in Hybrid Microgrid

In a hybrid microgrid, comprises a DC grid and an AC grid interlinked by a multi-objective control scheme of a bidirectional DC/AC converter. Bidirectional converters are crucial in hybrid microgrids because they enable two-way energy flow between various energy sources, storage systems, and the grid. They allow for efficient charging and discharging of batteries, facilitate seamless integration of renewable energy sources, and support grid stability by regulating voltage and frequency. By managing energy storage and distribution flexibly, bidirectional converters enhance the reliability, efficiency, and resilience of hybrid microgrids. Interlinking Converter (ILC) is a key component to connect the AC sub grid and DC sub grid. Its control strategy significantly affects power flow management, power quality, system efficiency and stability.

In microgrids, the primary or local level control is implemented for solar and battery for maintaining stable DC bus voltage. DC-DC Boost converters are being used as power converters in between load and source to enforce and increase the PV depending on the voltage output signal. The secondary or system level control is implemented by controlling the interlinking converter placed between ac and dc buses to supply stable voltage along with the smooth grid synchronization and ensuring the proper real power sharing between DC/AC buses. Furthermore, the ILC control prevents any negative sequence currents from flowing into the AC source.

4.3.1 Role of DC-DC Boost converter with MPPT in HMG

A boost converter is a DC/DC power converter which steps up voltage from its input (source) to its output (load). In continuous conduction mode (current through the inductor never falls to zero), it play a crucial role in increasing the voltage output from the maximum power point tracking system (Chen & Wang, 2019). These boost converters are responsible for efficiently converting the harvested solar energy into a higher voltage output, which is necessary for charging batteries or powering devices that require a higher voltage (Nguyen et al., 2020). Furthermore, the boost converters also help in maintaining a stable and regulated output voltage, thereby improving the overall efficiency and performance of the system as illustrated in Fig. 4.

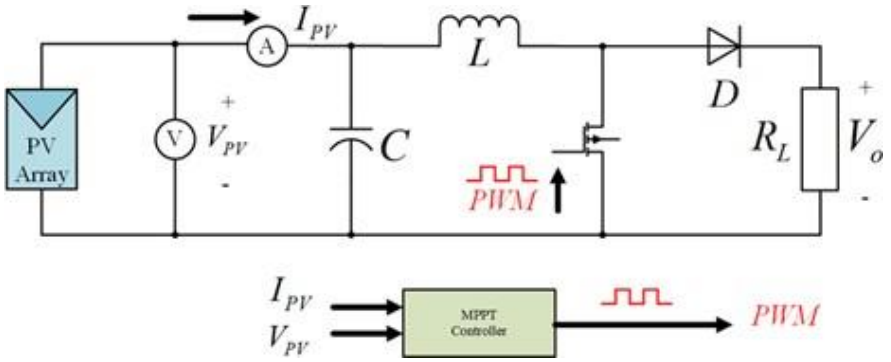

Fig.4. Circuit diagram of DC-DC Boost Converter

The boost converter output-input voltage relationship is proportional to the duty cycle in the sense that higher D will yield higher output voltages for a given input voltage. If the input voltage is Vin and the output voltage is Vout, Vout/Vin= 1/(1-D), where 0≤ D≤ 100% and D is the Duty cycle. In this case study, the power output of PV panel is 2000W, so the maximum operating power of the converter is 2000 W. Output voltage of the panel is 200 V at its MPP. The design parameters are the inductance, capacitance (supply) and capacitance (Load) are chosen as L=0.15H, C=100 and 470 uF and Vin=200V, Vout=400V, the voltage conversion ratio is set at K=400/200=2, frequency is 2.5 kHz, Load resistance is 80Ω. The algorithm proposed for MPPT in this manuscript, and detailed in the previous section, mainly focuses on the operating voltage and its corresponding power deviation. If the difference in power is positive, the future perturbation should follow suit to obtain MPP. Conversely, if the deviation in power is negative, the perturbation should be reversed and move in a reverse direction to obtain MPP. This procedure continues until it achieves maximum power.

4.4 Role of Bi-Directional DC/AC Converters in Hybrid Microgrid

Bidirectional converters are versatile power electronic devices that facilitate the flow of electrical energy in both directions between different parts of a power system. Unlike traditional unidirectional converters, which allow energy to flow in a single direction, bidirectional converters can switch between converting AC to DC and DC to AC, or between different DC voltage levels. This dual functionality is crucial in modern electrical systems, particularly in applications involving renewable energy sources and energy storage systems.

In renewable energy systems, bidirectional converters enable the integration of sources like solar panels and wind turbines with battery storage, allowing energy to be stored when production exceeds demand and later retrieved when needed. They also support grid stability by managing energy exchanges between microgrids and the main grid, helping balance supply and demand.

To validate the fuzzy logic-based control technique implemented in this proposed HMG, we had to design a bidirectional DC–AC converter that was capable of functioning as both an inverter and a PFC rectifier. The transition between these two modes of operation needed to be fully automated and without human intervention for our HMG to autonomously store, produce and supply energy for domestic use. Before validating its operation by appropriate experimental measurements, it is essential to detail the operating modes of the converter, as well as its control strategies. The energy transfer between a DC voltage source and an AC voltage source, and vice versa, was the basis of this structure. The association in series of a DC–DC stage and a DC–AC stage ensured this principle of operation with these two stages being necessarily bidirectional. The DC–DC stage needed to generate a rectified sine wave from the PWM command of the power switches. Since the power devices in this stage switched at a frequency of a few hundred kilohertz to optimize the compactness of the whole converter, the inductance, noted L1 was sized so that the ripple of the current was negligible com- pared to the sinusoidal component at low frequency (in this case, 50 Hz). Therefore, the DC–DC converter acted as a controllable output voltage source. By changing the voltage of a modulation stage, the output current could be regulated. This is very interesting, especially when the output current is strongly reduced or in the of variable DC voltage. This strategy allowed the output voltage of the DC–DC stage to be modulated. Specifically, when this modulated voltage was higher than the mains voltage, the

output current had a positive value. In the opposite case, the output current was negative. The design approach that was chosen allowed the converter to be used in both grid-connected and off-grid modes. Since the microcontroller was synchronized with the AC grid to sensibly drive the DC–DC and DC–AC stages, only the grid-connected mode will be discussed in the remainder of this paper. In this section of the paper, we will describe the control strategies of the pro- posed bidirectional DC–AC converter. We will only give the principles and thus, we will not detail the control circuit or the AC network connection strategy because several patents are pending. The DC–AC stage was controlled by the very same signal as the inverter mode, so it was synchronized with the AC grid at a frequency of 50 Hz.

Overall, bidirectional converters are essential for enhancing the flexibility, efficiency, and reliability of modern power systems, playing a key role in the transition to more sustainable and resilient energy infrastructures.

4.4.1 ILC Droop Control Coefficient

This paper proposes a novel, generalized droop scheme of ILC for autonomous power-sharing and control of a hybrid microgrid. A standalone hybrid microgrid is considered where the control of active power is more complex as compared to the grid-connected mode. The AC microgrid operates on frequency droop while voltage droop is used in the DC microgrid. A 3-dimensional plane is proposed for ILC control where the axis corresponds to DC voltage, AC frequency and converter power. The converter utilizes frequency droop at the AC terminal and voltage droop at the DC terminal so any change in DC voltage or AC frequency results in active power flow from an underloaded to the overloaded grid. The three quantities, namely active power, AC frequency and DC voltage, are introduced in the outer control loop of the converter along with three scaling factors which define the converter frequency and voltage droop.

To enable autonomous power-sharing between AC and DC grids, DC voltage droop and AC frequency droop are implemented in the outer control loop of the converter. Any load change in the ac grid will result in frequency variation and the power flow through the converter will change according to the frequency droop. Similarly, any dc load change will result in voltage variation which will change the converter power according to the dc voltage droop. Taking into account the fact that the converter does not generate any power and neglects converter losses, the following relation can be established.

$$k_1\Delta V_{dc} + k_2\Delta P_c - k_3\Delta f = 0 \tag{01}$$

Further expansion of this expression yields:

$$k_1\Delta V_{dc} + k_2 P_c - k_3 f - \left(k_1 V_{dc,ref} + k_2 P_{c,ref} - k_3 f_{ref}\right) \tag{02}$$

This is the generalized droop control which combines dc voltage and ac frequency. The maximum power flow through the tie line between ac and dc grids is represented as $P_{c,ref}$. The droop coefficients define the power flow through the converter. Equation (02) is a plane $ax + by + cz + d = 0$ drawn on the axis. If k_1 is set to zero, the converter operates in frequency droop and the droop coefficient is set by the ratio of k_2 and k_3 as shown in (03). This droop line is drawn on the plane on $f - P_c$ axis. In this case, no change in active power is observed due to load change in the dc grid and converter power is only dependent on ac grid frequency.

$$\frac{\Delta f}{\Delta P_c} = \frac{k_2}{k_3} \tag{03}$$

A voltage-frequency droop can be established by setting k_2 zero. In this case, the droop coefficient is given by

$$\frac{\Delta V_{dc}}{\Delta f} = \frac{k_3}{k_1} \tag{04}$$

This droop coefficient is the slope of the line drawn on $V_{dc} - f$ axis on the plane. Any change in DC voltage is translated into a change in frequency of ac grid but there is no control on the active power flowing through the converter. Any change in AC grid load will vary the power generated by the AC grid and the power flow through the converter according to the following relation:

$$\Delta P_L = \Delta P_{g,ac} - \Delta P_c \tag{05}$$

The load change in the ac sub-grid will cause frequency change. According to frequency droop, the change in ac power generation due to a change in frequency is given by:

$$\Delta P_{g,ac} = \frac{2\pi}{m}\Delta f \tag{06}$$

From the control scheme of the converter, the total change in active power ΔP_c from AC grid to DC grid is given by:

$$\Delta P_c = \frac{k_3\Delta f - k_1\Delta V_{dc}}{k_2} \tag{07}$$

Substituting Eqns.(06) and (07) in Eqn (05) gives us:

$$\Delta P_L = \frac{2\pi}{m}\Delta f - \frac{k_3\Delta f - k_1\Delta V_{dc}}{k_2} \quad (08)$$

This equation describes the impact of the ac load change on AC frequency and DC voltage in a hybrid microgrid. The change in power consumed by DC load can then be expressed as:

$$\Delta P_L = \frac{\Delta V_{dc}}{n} + \frac{k_3\Delta f - k_1\Delta V_{dc}}{k_2} \quad (09)$$

This relation can be used to determine its effect on frequency and DC voltage. Different voltage and frequency control strategies have been successfully implemented within AC and DC grids, but the control of hybrid microgrids requires further attention with a focus on ILC. In summary, interlinking converters are essential in microgrids as they allow for the integration of different energy sources, optimize power flow, enable power transfer between voltage systems, and ensure grid stability.

4.5 Controller Design

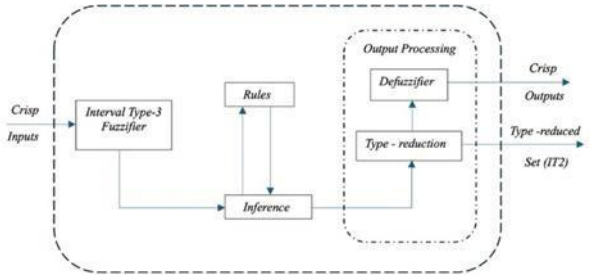

Fig. 5. Block Diagram of Interval Type-3 Fuzzy Controller

The voltage and frequency of MGs are strongly impressionable from the active and reactive load fluctuations. A change in load leads to an imbalance between generation and consumption. The output voltage and frequency of the DGs are primarily controlled by the droop characteristics. But, in case of severe changes in load, the DGs may be failed and the Microgrid is collapsed. Subsequently, the research proposed the interval type 3 fuzzy controller is used for controlling the load frequency of the multi-area system. A 1% step load perturbation is applied to the load demand of the power plant and analysis of the system responses in terms of settling time, peak overshoot and peak undershoot. Henceforth, it is necessary to maintain the system frequency to be constant. The structure of an interval type-3 system is almost the same as for type-2 and type-1, and it is composed of a fuzzifier, rules, inference, type reduction and defuzzifier [36]. In Fig. 5 we show the structure of an interval IT3 system [33,34,35].

Implementing an Interval Type-3 Fuzzy Controller in MATLAB involves defining fuzzy sets, membership functions, a rule base, and processes for fuzzification, inference, and defuzzification. Below is a basic outline ,

Step 1: Define Membership Functions

First, define the primary and secondary membership functions.

```
" function mu = primary_membership_function(x, a, b, c)
% Triangular membership function
mu = max(min((x - a) / (b - a), (c - x) / (c - b)), 0);
end

function mu = secondary_membership_function(primary_mu, l, u)
% Secondary membership function as a simple linear combination
mu = (primary_mu * (u - l)) + l;
end "
```

Step 2: Fuzzification

Convert crisp inputs into fuzzy values using the membership functions.

```
" function fuzzy_values = fuzzify(input_value, membership_functions)
  fuzzy_values = zeros(1, length(membership_functions));
```

```
    for i = 1:length(membership_functions)
        fuzzy_values(i) = membership_functions{i}(input_value);
    end
end"
```

Step 3: Rule Base

Define a set of fuzzy rules and apply them.

```
" function output_fuzzy_values = rule_base(input_fuzzy_values)
    % Example: simple rule base with two rules
    rule1 = min(input_fuzzy_values(1), input_fuzzy_values(2));
    rule2 = min(input_fuzzy_values(3), input_fuzzy_values(4));
    output_fuzzy_values = [rule1, rule2];
end"
```

Step 4: Inference

Apply the fuzzy rules to determine the output fuzzy sets.

```
" function inference_result = inference(fuzzy_values, rule_base)
inference_result = zeros(1, length(rule_base));
for i = 1:length(rule_base)
inference_result(i) = rule_base(i);
end
end"
```

Step 5: Defuzzification

Convert the fuzzy output sets back into crisp values.

```
"function crisp_output = defuzzify(fuzzy_output_values)
% Example: centroid method
numerator = sum(fuzzy_output_values);
denominator = length(fuzzy_output_values);
crisp_output = numerator / denominator;
end"
```

This is a simplified implementation to demonstrate the basic structure of an Interval Type-3 Fuzzy Controllerin MATLAB. A real-world implementation would require more detailed handling of the secondary member- ship functions, more complex rule definitions, and more sophisticated methods for fuzzification, inference, and defuzzification.

4.5.1 Interval Type 3 Fuzzy Controller

The interval type-3 FLSs (IT3-FLSs) are developed to handle more levels of uncertainty. In this study, IT3-FLSs are used for online dynamic identification. as Illustrated in Fig. 5,The structure of IT3-FLS is explained step-by-step below:

The inputs of IT3-FLSs are $y_1 = I_p(t)$, $y_2 = V_c(t-\tau)$, $y_3 = I_b(t)$, where, I_p and I_b are the currents of PV and battery, respectively and V_c is the load voltage. τ represents the sample time.

For each input, two Gaussian membership functions (MFs) are considered. The centres of MFs are set to the upper and lower bounds of each input. For input I_p, $\tilde{A}^2_{I_p}$, respectively. Similarly, for input I_b, one has: the upper and lower memberships are obtained as:

$$\bar{\mu}_{\tilde{A}^1_{I_p}|\alpha}(I_p) = exp\left(-\frac{\left(I_p - \underline{c}_{\tilde{A}^1_{I_p}}\right)^2}{\bar{\sigma}^2_{\tilde{A}^1_{I_p}|\alpha}}\right) \tag{10}$$

$$\bar{\mu}_{\tilde{A}_{I_p}^2|\alpha}(I_p) = exp\left(-\frac{\left(I_p-\bar{c}_{\tilde{A}_{I_p}^2}\right)^2}{\bar{\sigma}^2_{\tilde{A}_{I_p}^2|\alpha}}\right) \tag{11}$$

$$\underline{\mu}_{\tilde{A}_{I_p}^1|\alpha}(I_p) = exp\left(-\frac{\left(I_p-\underline{c}_{\tilde{A}_{I_p}^1}\right)^2}{\underline{\sigma}^2_{\tilde{A}_{I_p}^1|\alpha}}\right) \tag{12}$$

$$\underline{\mu}_{\tilde{A}_{I_p}^2|\alpha}(I_p) = exp\left(-\frac{\left(I_p-\bar{c}_{\tilde{A}_{I_p}^2}\right)^2}{\underline{\sigma}^2_{\tilde{A}_{I_p}^2|\alpha}}\right) \tag{13}$$

Where, α is the level of the horizontal slice. $\tilde{A}_{I_p}^1$ and $\tilde{A}_{I_p}^2$ are the first and second MFs for input I_p. $\underline{c}_{\tilde{A}_{I_p}^1}$ and $\bar{c}_{\tilde{A}_{I_p}^2}$ are the centres of $\tilde{A}_{I_p}^1$ and $\tilde{A}_{I_p}^2$, respectively. $\bar{\sigma}_{\tilde{A}_{I_p}^1|\alpha}/\underline{\sigma}_{\tilde{A}_{I_p}^1|\alpha}$ and $\bar{\sigma}_{\tilde{A}_{I_p}^2|\alpha}/\underline{\sigma}_{\tilde{A}_{I_p}^2|\alpha}$ are the standard division for the upper/lower bounds of $\tilde{A}_{I_p}^1$ and $\tilde{A}_{I_p}^2$, respectively. Similarly, for input I_b, one has:

$$\bar{\mu}_{\tilde{A}_{I_b}^1|\alpha}(I_b) = exp\left(-\frac{\left(I_b-\underline{c}_{\tilde{A}_{I_b}^1}\right)^2}{\bar{\sigma}^2_{\tilde{A}_{I_b}^1|\alpha}}\right) \tag{14}$$

$$\bar{\mu}_{\tilde{A}_{I_b}^2|\alpha}(I_b) = exp\left(-\frac{\left(I_b-\bar{c}_{\tilde{A}_{I_b}^2}\right)^2}{\bar{\sigma}^2_{\tilde{A}_{I_b}^2|\alpha}}\right) \tag{15}$$

$$\underline{\mu}_{\tilde{A}_{I_b}^1|\alpha}(I_b) = exp\left(-\frac{\left(I_b-\underline{c}_{\tilde{A}_{I_b}^1}\right)^2}{\underline{\sigma}^2_{\tilde{A}_{I_b}^1|\alpha}}\right) \tag{16}$$

$$\underline{\mu}_{\tilde{A}_{I_b}^2|\alpha}(I_b) = exp\left(-\frac{\left(I_b-\bar{c}_{\tilde{A}_{I_b}^2}\right)^2}{\underline{\sigma}^2_{\tilde{A}_{I_b}^2|\alpha}}\right) \tag{17}$$

Where, $\tilde{A}_{I_b}^1$ and $\tilde{A}_{I_b}^2$ are the first and second MFs for input Ib. $\underline{c}_{\tilde{A}_{I_b}^1}$ and $\bar{c}_{\tilde{A}_{I_b}^2}$ are the centres of $\tilde{A}_{I_b}^1$ and $\tilde{A}_{I_b}^2$, respectively. $\bar{\sigma}_{\tilde{A}_{I_b}^1|\alpha}/\underline{\sigma}_{\tilde{A}_{I_p}^1|\alpha}$ and $\bar{\sigma}_{\tilde{A}_{I_b}^2|\alpha}/\underline{\sigma}_{\tilde{A}_{I_b}^2|\alpha}$ are the standard division for the upper/lower bounds of $\tilde{A}_{I_b}^1$ and $\tilde{A}_{I_b}^2$, respectively. Finally, for input V_c, one has:

$$\bar{\mu}_{\tilde{A}_{V_c}^1|\alpha}(V_c) = exp\left(-\frac{\left(V_c-\underline{c}_{\tilde{A}_{V_c}^1}\right)^2}{\bar{\sigma}^2_{\tilde{A}_{V_c}^1|\alpha}}\right) \tag{18}$$

$$\bar{\mu}_{\tilde{A}_{V_c}^2|\alpha}(V_c) = exp\left(-\frac{\left(V_c-\bar{c}_{\tilde{A}_{V_c}^2}\right)^2}{\bar{\sigma}^2_{\tilde{A}_{V_c}^2|\alpha}}\right) \tag{19}$$

$$\underline{\mu}_{\tilde{A}_{V_c}^1|\alpha}(V_c) = exp\left(-\frac{\left(V_C-\underline{c}_{\tilde{A}_{V_c}^1}\right)^2}{\underline{\sigma}^2_{\tilde{A}_{V_c}^1|\alpha}}\right) \tag{20}$$

$$\underline{\mu}_{\tilde{A}_{V_c}^2|\alpha}(V_c) = exp\left(-\frac{\left(V_c-\bar{c}_{\tilde{A}_{V_c}^2}\right)^2}{\underline{\sigma}^2_{\tilde{A}_{V_c}^2|\alpha}}\right) \tag{21}$$

Where, $\tilde{A}_{V_c}^1$ and $\tilde{A}_{V_c}^2$ are the first and second MFs for input V_c. $\underline{c}_{\tilde{A}_{V_c}^1}$ and $\bar{c}_{\tilde{A}_{V_c}^2}$ are the centres of $\tilde{A}_{V_c}^1$ and $\tilde{A}_{V_c}^2$, respectively. $\bar{\sigma}_{\tilde{A}_{V_c}^1|\alpha}/\underline{\sigma}_{\tilde{A}_{V_c}^1|\alpha}$ and $\bar{\sigma}_{\tilde{A}_{V_c}^2|\alpha}/\underline{\sigma}_{\tilde{A}_{V_c}^2|\alpha}$ are the standard division for the upper/lower bounds of $\tilde{A}_{V_c}^1$ and $\tilde{A}_{V_c}^2$, respectively. 3) The output of $\hat{f}_1$ and $\hat{f}_2$ are:

$$\hat{f}_1 = \theta_1^T\zeta_1 \tag{22}$$

$$\hat{f}_2 = \theta_2^T\zeta_2 \tag{23}$$

Where, θ_i and ζ_i are:

$$\theta_i = \left[\underline{w}_{i1}, \dots, \underline{w}_{iR}, \overline{w}_{i1}, \dots, \overline{w}_{iR}\right]^T \tag{24}$$

$$\zeta_i = \left[\underline{\zeta}_{i1}, \dots, \underline{\zeta}_{iR}, \bar{\zeta}_{i1}, \dots, \bar{\zeta}_{iR}\right]^T \tag{25}$$

Where, $\overline{w}_{i1}$ and $\underline{w}_{i1}$ are the parameters of $l-$th rule for $i-$th IT3-FLS and R represents the number of rules. $\underline{\zeta}_{i1}$ and $\bar{\zeta}_{i1}$ are:

$$\bar{\zeta}_l = \frac{\sum_{j=1}^{n_\alpha} \bar{\alpha}_j \frac{\bar{z}^l_{\mu s=\bar{\alpha}_j}}{\sum_{l=1}^{R}\left(\bar{z}^l_{\mu s=\bar{\alpha}_j} + \underline{z}^l_{\mu s=\bar{\alpha}_j}\right)}}{\sum_{j=1}^{n_\alpha}(\bar{\alpha}_j + \underline{\alpha}_j)} + \frac{\sum_{j=1}^{n_\alpha} \underline{\alpha}_j \frac{\bar{z}^l_{\mu s=\underline{\alpha}_j}}{\sum_{l=1}^{R}\left(\bar{z}^l_{\mu s=\underline{\alpha}_j} + \underline{z}^l_{\mu s=\underline{\alpha}_j}\right)}}{\sum_{j=1}^{n_\alpha}(\bar{\alpha}_j + \underline{\alpha}_j)}, \; l = 1, \dots 8 \tag{26}$$

$$\underline{\zeta}_l = \frac{\sum_{j=1}^{n_\alpha} \bar{\alpha}_j \frac{\underline{z}^l_{\mu s=\bar{\alpha}_j}}{\sum_{l=1}^{R}\left(\bar{z}^l_{\mu s=\bar{\alpha}_j} + \underline{z}^l_{\mu s=\bar{\alpha}_j}\right)}}{\sum_{j=1}^{n_\alpha}(\bar{\alpha}_j + \underline{\alpha}_j)} + \frac{\sum_{j=1}^{n_\alpha} \underline{\alpha}_j \frac{\underline{z}^l_{\mu s=\underline{\alpha}_j}}{\sum_{l=1}^{R}\left(\bar{z}^l_{\mu s=\underline{\alpha}_j} + \underline{z}^l_{\mu s=\underline{\alpha}_j}\right)}}{\sum_{j=1}^{n_\alpha}(\bar{\alpha}_j + \underline{\alpha}_j)}, \; l = 1, \dots 8 \tag{27}$$

Where, n_α is the number of horizontal slices and:

$$\underline{\zeta}_l = \frac{\sum_{j=1}^{n_\alpha} \bar{\alpha}_j \frac{\underline{z}^l_{\mu s=\bar{\alpha}_j}}{\sum_{l=1}^{R}\left(\bar{z}^l_{\mu s=\bar{\alpha}_j} + \underline{z}^l_{\mu s=\bar{\alpha}_j}\right)}}{\sum_{j=1}^{n_\alpha}(\bar{\alpha}_j + \underline{\alpha}_j)} + \frac{\sum_{j=1}^{n_\alpha} \underline{\alpha}_j \frac{\underline{z}^l_{\mu s=\underline{\alpha}_j}}{\sum_{l=1}^{R}\left(\bar{z}^l_{\mu s=\underline{\alpha}_j} + \underline{z}^l_{\mu s=\underline{\alpha}_j}\right)}}{\sum_{j=1}^{n_\alpha}(\bar{\alpha}_j + \underline{\alpha}_j)}, \; l = 1, \dots R \tag{28}$$

The rules are written as:

Rule #1: If I_p is $\tilde{A}^1_{I_p}|\alpha$ and I_b is $\tilde{A}^1_{I_b}|\alpha$ and V_c is $\tilde{A}^1_{V_c}|\alpha$
Then $\hat{f}_i \in [\underline{w}_{i1}, \overline{w}_{i1}]$
Rule #2: If I_p is $\tilde{A}^1_{I_p}|\alpha$ and I_b is $\tilde{A}^1_{I_b}|\alpha$ and V_c is $\tilde{A}^2_{V_c}|\alpha$
Then $\hat{f}_i \in [\underline{w}_{i2}, \overline{w}_{i2}]$
Rule #3: If I_p is $\tilde{A}^1_{I_p}|\alpha$ and I_b is $\tilde{A}^2_{I_b}|\alpha$ and V_c is $\tilde{A}^1_{V_c}|\alpha$
Then $\hat{f}_i \in [\underline{w}_{i3}, \overline{w}_{i3}]$
Rule #4: If I_p is $\tilde{A}^1_{I_p}|\alpha$ and I_b is $\tilde{A}^2_{I_b}|\alpha$ and V_c is $\tilde{A}^2_{V_c}|\alpha$
Then $\hat{f}_i \in [\underline{w}_{i4}, \overline{w}_{i4}]$
Rule #5: If I_p is $\tilde{A}^2_{I_p}|\alpha$ and I_b is $\tilde{A}^1_{I_b}|\alpha$ and V_c is $\tilde{A}^1_{V_c}|\alpha$
Then $\hat{f}_i \in [\underline{w}_{i5}, \overline{w}_{i5}]$
Rule #6: If I_p is $\tilde{A}^2_{I_p}|\alpha$ and I_b is $\tilde{A}^1_{I_b}|\alpha$ and V_c is $\tilde{A}^2_{V_c}|\alpha$
Then $\hat{f}_i \in [\underline{w}_{i6}, \overline{w}_{i6}]$
Rule #7: If I_p is $\tilde{A}^2_{I_p}|\alpha$ and I_b is $\tilde{A}^2_{I_b}|\alpha$ and V_c is $\tilde{A}^1_{V_c}|\alpha$
Then $\hat{f}_i \in [\underline{w}_{i7}, \overline{w}_{i7}]$
Rule #8: If I_p is $\tilde{A}^2_{I_p}|\alpha$ and I_b is $\tilde{A}^2_{I_b}|\alpha$ and V_c is $\tilde{A}^2_{V_c}|\alpha$
Then $\hat{f}_i \in [\underline{w}_{i8}, \overline{w}_{i8}]$

In the type-3 MFs, the secondary membership is not a crisp value but it is a fuzzy set. Also a horizontal slice of a level $\mu_s = \alpha_k$ is equal with two slices at levels $\mu_s = \underline{\alpha}_k$ and $\mu_s = \overline{\alpha}_k$ in type-2 counterpart. Consequently, the research proposed a swarm-based hybrid metaheuristic optimizer of the Bacterial Foraging Optimization Algorithm (BFOA) which optimally tunes and controls the fuzzy controller parameters.

4.3.2 Enhanced Controller efficiency by BFOA

Initiating the deployment of the Bacterial Foraging Optimization Algorithm to refine the operations of a fuzzy type-3 controller within a microgrid framework involves a sequence of strategic steps. Commence with the construction of a detailed microgrid model encapsulating its integral components—distributed generation units,

storage mechanisms, consumer loads, and command modules. Forge a sophisticated fuzzy type-3 controller, crafted to govern the intricacies of power distribution, voltage modulation, and frequency stabilization, pinpointing the specific variables that warrant enhancement. Subsequently, establish a robust objective function adept at evaluating the microgrid's operational efficacy, engaging metrics that aim to curtail energy dissipation, equilibrate supply-demand dynamics, fortify voltage constancy, and augment frequency adherence. Proceed to meticulously calibrate the BFOA configurations, setting parameters such as bacterial population foundation, chemotaxis stages, navigational duration, procreation sequencing, and the probability metrics for elimination and dispersal phases. Culminate by methodically applying the BFOA, refining the controller parameters through iterative optimization, assiduously informed by the designated objective function's feedback, to realize an apex in microgrid performance (Das et al., 2009) (Hu et al., 2020)

4.3.2.1 Pseudo-code for BFOA-based Optimization

Initialize microgrid model and fuzzy type-3 controller parameters
Define objective function F(x) to evaluate microgrid performance

Initialize BFOA parameters:
S (number of bacteria)
Nc (number of chemotactic steps)
Ns (swim length)
Nre (number of reproduction steps)
Ned (number of elimination-dispersal events)
Ped (elimination-dispersal probability)

Initialize bacteria positions randomly in the search space

FOR each elimination-dispersal event
FOR each reproduction step
FOR each chemotactic step
FOR each bacterium i

Compute the objective function F(x) for current position

Tumble: generate a random direction Δ(i)
Move: compute new position using Δ(i)

Compute F(x) at new position

WHILE (not better or swim length not exceeded)
Move in the same direction and compute F(x)
END WHILE
END FOR

Implement swarming behavior

END FOR
Sort bacteria based on objective function value
Reproduce: eliminate least healthy half and split the healthier half
END FOR
Eliminate and disperse bacteria with probability Ped
END FOR
Output the optimized fuzzy type-3 controller parameters
Apply optimized controller to the microgrid and validate performance

By integrating the optimized parameters into the fuzzy type-3 controller and simulating the microgrid operation, you can validate the performance by comparing it against predefined benchmarks or previous configurations. If necessary, iterate the optimization process, adjusting the BFOA parameters for improved results and leading to enhanced system performance and stability.

However, most fuzzy controllers are static in that they respond only to current input, so they may not offer any improvement over the dynamic nature of designs. By replacing nonlinear and time-varying aspects of a neural network with uncertainties, a robust reinforcement learning procedure results that are guaranteed to remain stable even as the neural network is being trained.

4.6 Power Quality Analysis

In this study, a new reactive power control strategy is employed for optimization of the reactive power along with the stability improvement of the system under different small perturbed conditions. Therefore, this study focuses on controlling the reactive power of the hybrid power system model with the aid of a Static Synchronous Compensator (STATCOM). Further, evaluate the renewable energy resources' penetration limit of the AC-DC hybrid grid, which considers both economy and safety. The static stability indicators are considered for an evaluation of the penetration limit of RES.

4.6.1 Implementation of STATCOM as a Reactive Compensator

STATCOM is developed on the solid-state-based synchronous source of voltage which replicates a synchronous machine of ideal nature. It generates a set of 3-phase balanced sinusoidal voltages at the fundamental frequency by continuous controlling of phase angle and amplitude. The schematic of the STATCOM and its equivalent structure has been given in Fig. 6. A illustrated in Fig. 6, the voltage source converter, DC capacitor, and coupling transformer. The real part of the STATCOM controller current is insignificant and considered zero. The reactive current can be controlled by the variation of α and δ.

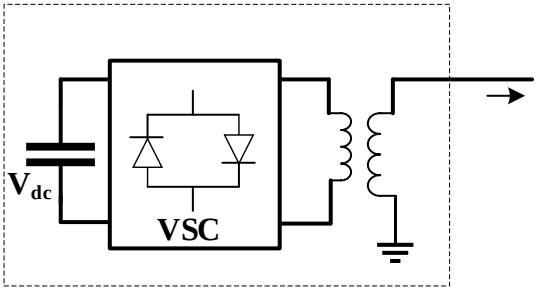

Fig. 6: Schematic Diagram for STATCOM Configuration

In this paper, α is the STATCOM's fundamental output voltage (kV_{dc}) phase angle and δ is the phase angle of the system bus voltage, U where the STATCOM is connected. The amplitude of the converter's fundamental output voltage is $kU_{dc}$where U_{dc}represents DC voltage developed in between the DC capacitor. The STATCOM controller injecting the reactive power to the connected bus has been given as in equation (30).

$$Q_{STATCOM} = kU_{dc}^2 B - kU_{dc} UB\ cos\ (\alpha - \delta) + kU_{dc} UG\ sin(\alpha - \delta) \quad (29)$$

In the considered HPS, bus voltage is taken as a reference voltage; so, the bus angle (δ) is zero. In the above equation, the G term is also insignificant, because $(G + jB)$ characterizes the admittance of the step-down transformer. Thus, equation (30) now becomes equation (31), considering G and δ as zero.

$$Q_{STATCOM} = kU_{dc}^2 B - kU_{dc} UB\ cos\alpha \quad (30)$$

Here, in equation (31), U and α, are the variable terms on which the reactive power depends; under the small perturbations, the change in reactive power of STATCOM can be written as equation (32).

$$\Delta Q_{STATCOM}(s) = G_1 \Delta\alpha(s) + G_2 \Delta U(s) \quad (31)$$

Where, $G_1 = kU_{dc}UB\ sin\alpha$ and $G_2 = kU_{dc}UB\ cos\alpha$.

It evaluates the renewable energy resources' penetration limit of the AC-DC hybrid grid, which considers both economy and safety. The static stability indicators are considered for an evaluation of the penetration limit of RES.

4.7 Loads, Energy storage Devices and utility Grid

DC Load: Devices that consume direct currents, such as DC machines, electric vehicles, and many electronic devices, are defined as DC loads. Similarly to the DC source, the DC load is represented as a controlled direct current source, but functions by absorbing power from the microgrid.

AC Load: The AC loads are represented by sets of impedance, composed of balanced three-phase resistors and inductances in series. Thus, these AC loads consume the active and reactive power of the AC microgrids (ACMG). The input and output of such loads occur according to the desired power profiles.

Nonlinear Load: The nonlinear load represents devices that distort the electrical current waveform, contaminating the grid with harmonic content. Such loads are modelled as a diode rectifier bridge with a resistive load and inductive filter at the input. The distortion in the waveform occurs due to the harmonic components added to the fundamental sinusoidal current. These harmonic distortions cause issues in the utility grid, thereby affecting the power quality of the energy supplied by the system.

Energy Storage Device: Among different existing energy storage technologies, Li-ion batteries are chosen as ESD in this work. The dynamic behaviour of such ESD is based on the Shepherd model, which represents the battery as a controlled DC source in series with internal resistance.

It is possible to describe, in a simplified way, the output voltage of the battery bank, according to equation (1).

$$V_{bat} = E_{bat} - R_{bat} I_{bat} \quad (32)$$

Where, V_{bat} and E_{bat} are the output and internal battery voltage, respectively; R_{bat} is the internal resistance, and I_{bat} is the battery's electrical current.

Utility Grid: Despite the main aspect of a microgrid being the possibility of operating in the standalone or grid-connected mode, this paper focuses exclusively on studying the grid-connected operation. In this study, the utility grid is implemented by a balanced, 60 Hz, three-phase, 220 V RMS, phase-to-phase AC source. Each voltage source represents a phase, with 120o of phase-shift between each phase, in the positive sequence. RL impedances are employed to characterize the conductors' dynamic effect, emulating the transmission line impedances. The value of these impedances is determined according to conventional short-circuit power for electrical distribution systems.

5. Simulation results

The simulation of the proposed hybrid microgrid involves modelling various components, integrating them into a unified system, and analysing performance under different operating conditions using MATLAB 2023a environment. The simulation is conducted on a Personal Computer System running Windows 11 Operating System with 6GB DDR3 of RAM and Intel Core i7 processor @ 3.5GHz. The total simulation time amounts to 10.190 seconds including power flow analysis and power quality evaluation at the DC-link of the DC Microgrid and the utility grid. The system includes loads and sources rated up to 4.5 kW, along with interlinkingconverters designed for a nominal power of 3 kW to ensure efficient hybrid power system operation based on selected inductors and capacitors which meet voltage ripple requirements as well as nominal power needs of the power converters. This accurate simulation models effectively analysing its performance under variousconditions using high-performance computer configurations advantageous in demonstrating successful integration of various components within this complex energy network while providing valuable insights into its feasibility showcasing effective component integration enabling smooth operations across diverse scenarios.

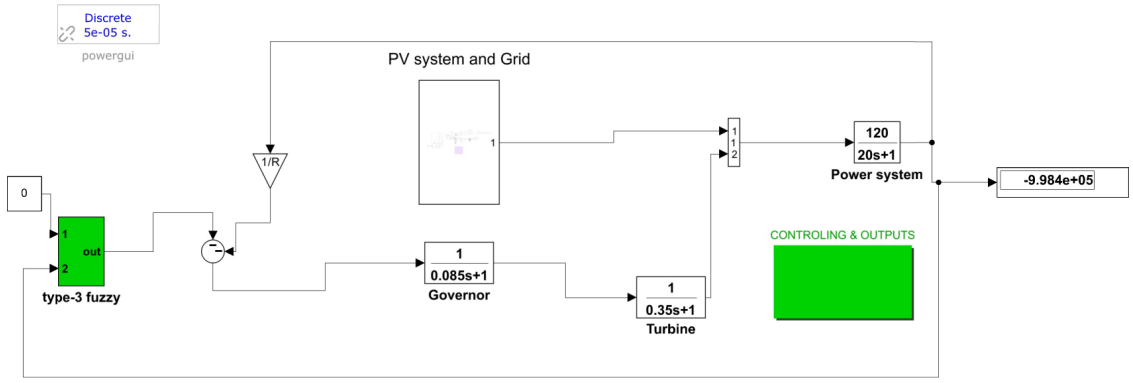

Fig.7. Simulation Model for Hybrid Renewable Energy Resources

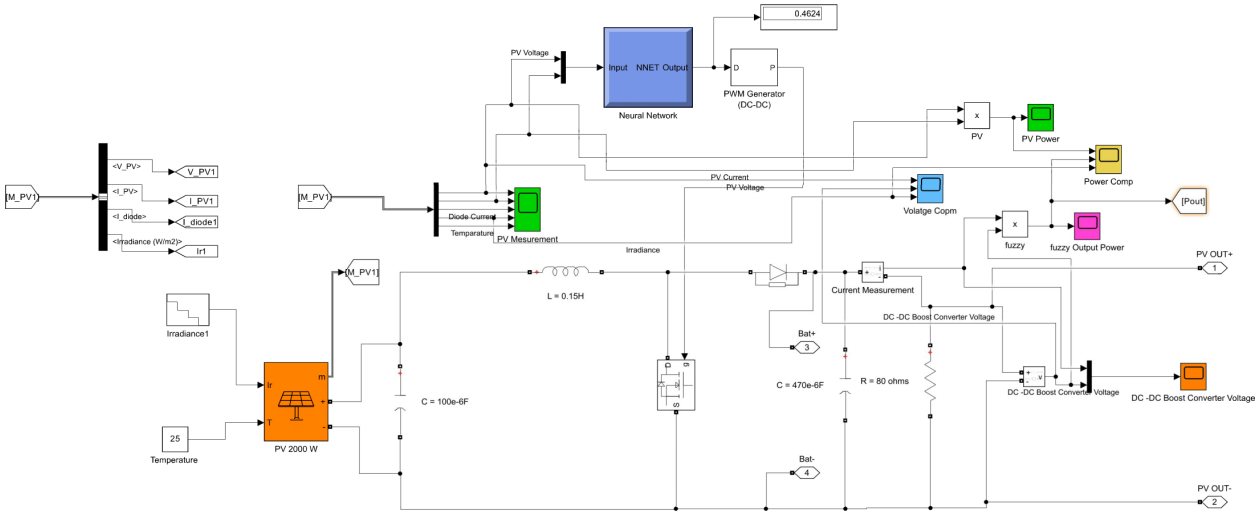

Fig. 8. Simulation Model of AI Based MPPT Scheme

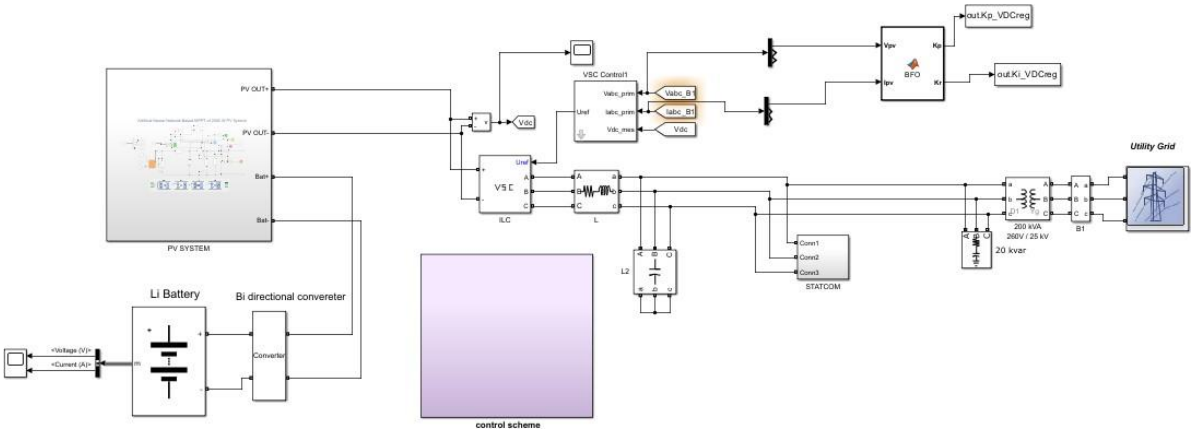

Fig.9. Proposed Simulation Model of PV system and Grid

The simulation model for hybrid renewable energy resources, illustrated in Fig. 7,8,9 was developed using MATLAB/Simulink. In this hybrid PV system, the PV array serves as the primary power source. Renewable energy sources are connected in parallel, with a battery connected across this parallel combination. The battery discharges when the voltage exceeds 30V and charges when the voltage drops below 30V. In this Battery circuit, if the semi-oxide concentration decreases linearly then the battery voltage drops rapidly.

The Key components in this model include the PV Panel with AI based MPPT, Type 3 fuzzy Controller, Bidi-rectional converter ,DC/DC converter, battery model, and power system. The optimum power control and pitch angle control mechanisms drive the induction generator. The turbine's external inputs are wind speed and rotor speed. The main

objective of the grid-side converter is to regulate the DC link capacitor voltage and control power flow between the DC bus and the AC side.

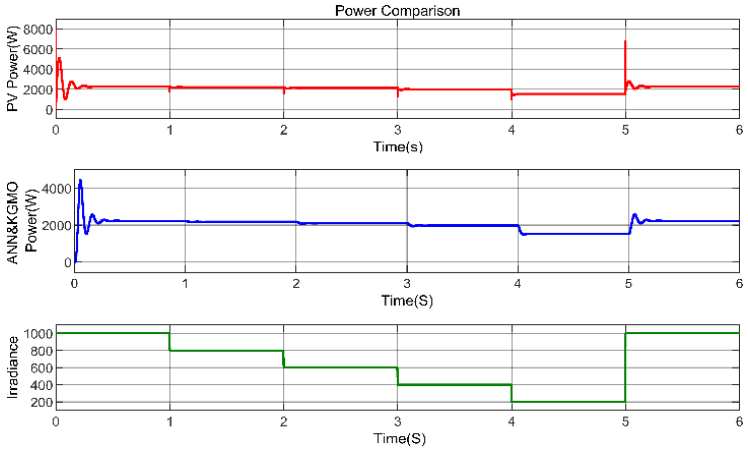

Fig. 10(a). Power Comparison from ANN-KGMO *method*

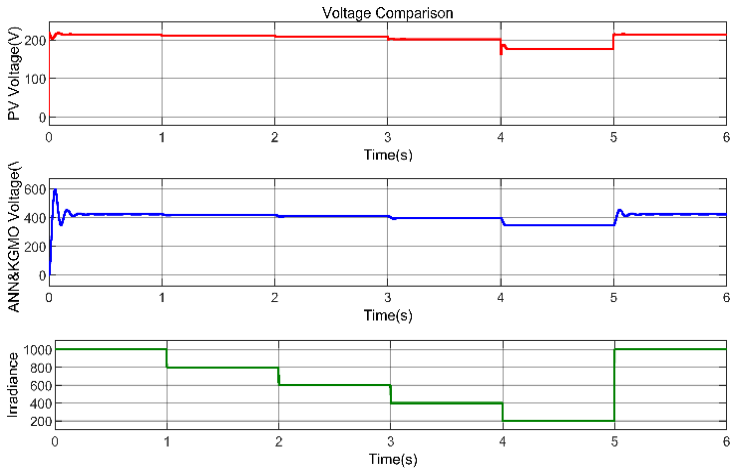

Fig. 10(b). Voltage Comparison from ANN-KGMO *method*

Fig. 10 shows the simulation outcome with ANN-KGMO based MPPT tracking algorithm is more reliable than the conventional control methods. It has less settling time with no steady state oscillations and more power output.

It is observed that ANN-KGMO based MPPT algorithm regulates the output voltage at 400V and hence the power at 2000 W with rapid step changes in the solar irradiance.

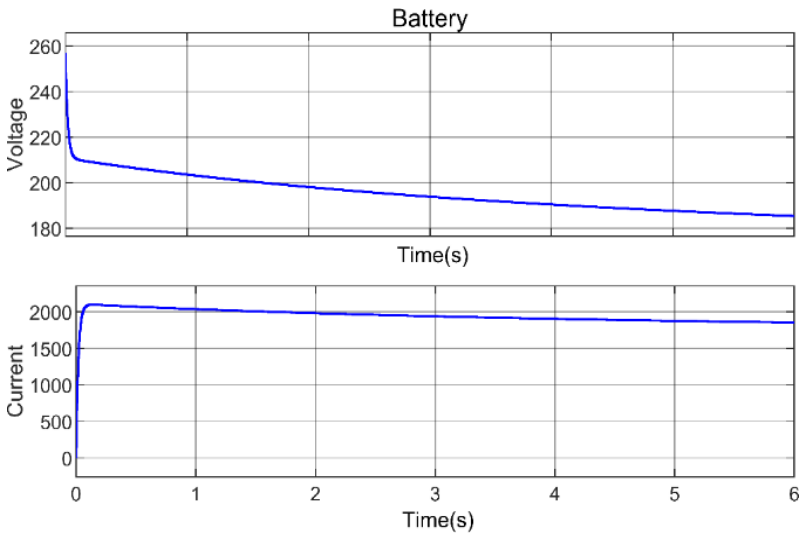

Fig.11. Current and Voltage Graph for Battery

The current and voltage graph for the battery is presented in Fig. 11. It produces a battery current of approximately 1900 A for 6 second. However, the voltage produced due to the battery is approximately 190 V for time 6 second. The input charging current to the battery stack in a photovoltaic hybrid solution will not be constant due to the atmospheric conditions and the time of day.

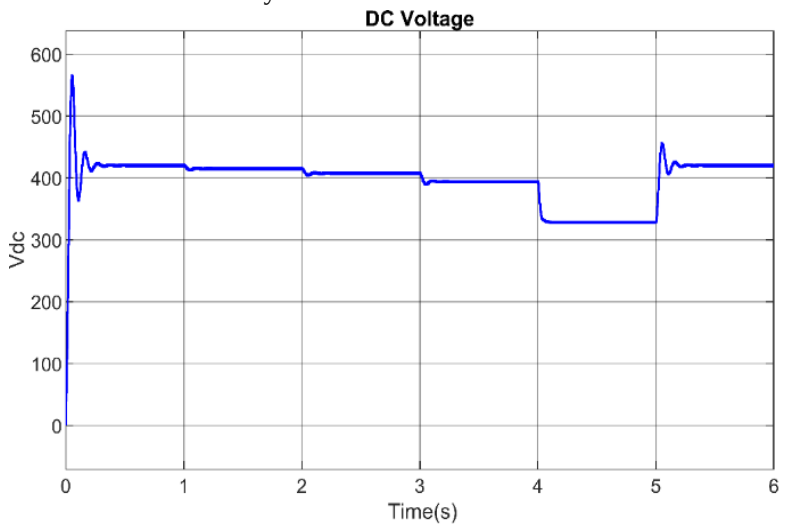

Fig.12. Response of Hybrid V_{dc} value

Fig. 12 the simulation results of ANN-KGMO methods and Battery DC Voltage at 25°C temperature and light intensity is varied from 1000 to 200 W/m^2 in steps at rate of 200 W/m^2 per second. After reaching 200 W/m^2 the intensity is varied to 1000W/m^2 in single step. Upto 4 sec (400 W/m^2) seconds the output voltage is maintained approximately 410V but after reaching 200 W/m^2 at 4 second the DC Voltage value reduced to 340V and gain the intensity is varied to 1000W/m^2 in single step the DC Voltage is reached to approximately 410V.

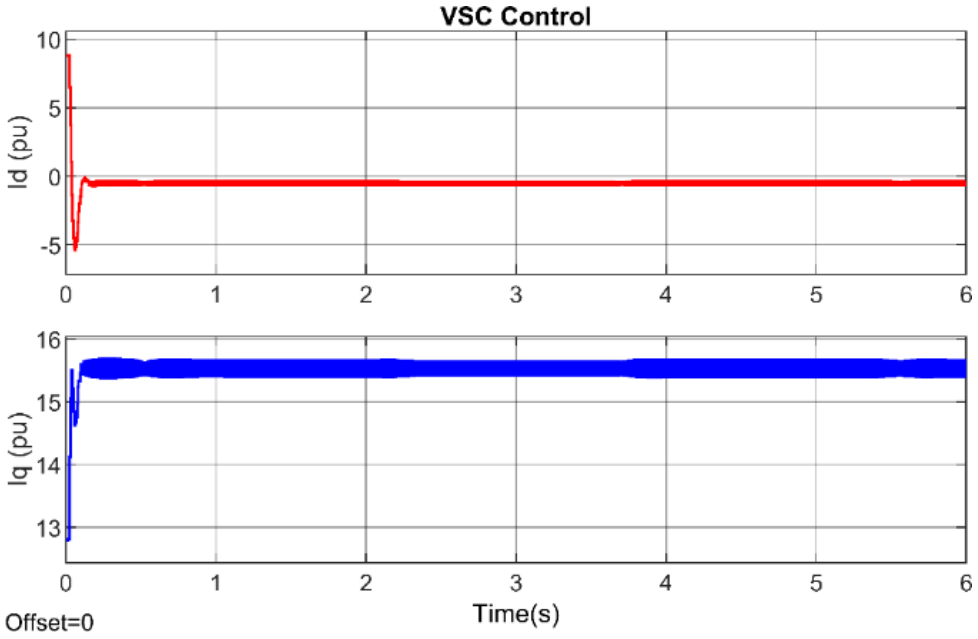

Fig.13. Response of I_d, I_q in VSC Conrol

Fig. 13. shows the high quality of the current injected into the grid with the proposed current control scheme. This result meets the requirements of the grid-connection standard. The grid voltage produces 1.9 X 10^4 V. The grid voltage harmonic disturbances are rejected by the robust ADRC controller, leading to much better performance.

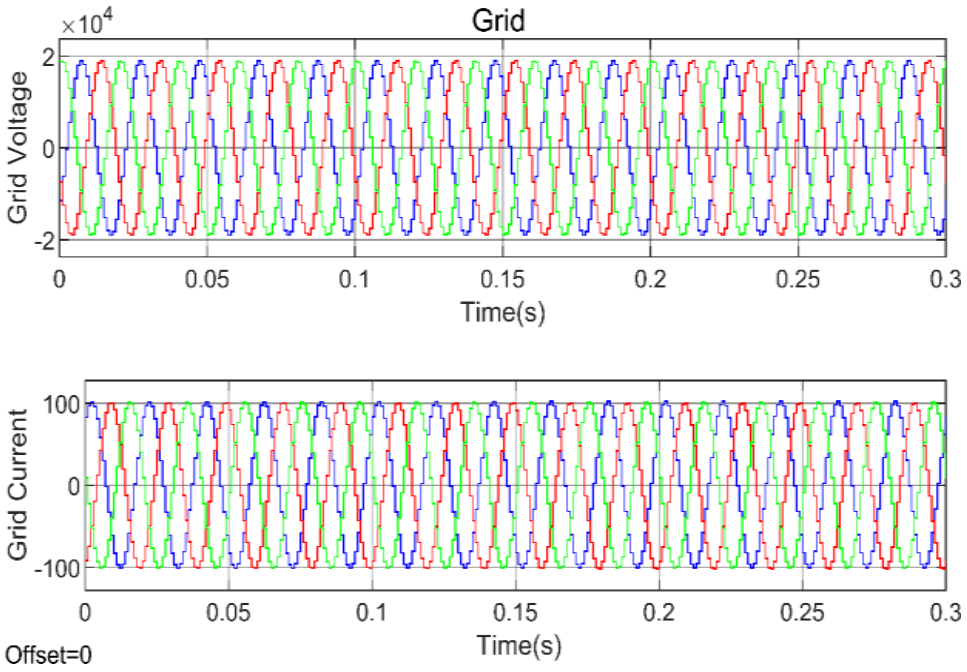

Fig.14. Grid Current and Grid Voltage

Fig. 14 reveals the grid current and grid voltage. The grid current is regulated to its nominal value and is in phase with the grid voltage as can be seen in Fig. 9. The grid voltage produces 1.9 X 10^4 V.

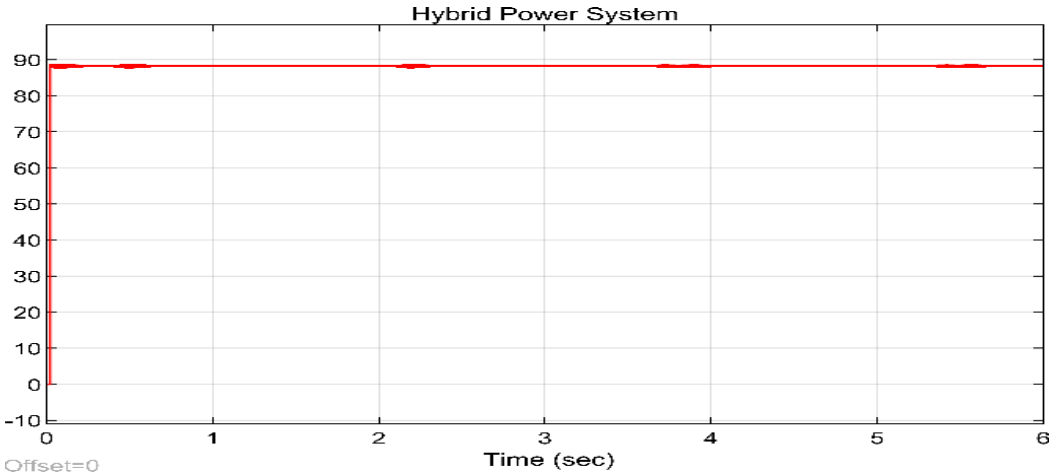

Fig.15. Response of Power for proposed hybrid power system

The power graph for the proposed hybrid power system is presented in Fig. 15. It produces approximately 90 kW of power generated from hybrid power systems. This power value is measured based on the time seconds. This reading of power was measured when the time was 0 to 6 second, respectively. The temperature is set at 25 degrees Celsius, and the light intensity is gradually reduced from 1000 to 200 W/m^2 at a rate of 200 W/m^2/s. After attaining 200 W/m2, the intensity is increased in one step to 1000 W/m2. The light intensity varied with respect to time but power generated by proposed hybrid power system was maintained constant that is approximately 90 kW.

Fig. 16 appearances PLL frequency and ω under different conditions. The frequency was maintained constant and Output 1: Measured frequency (Hz)=w/(2pi), Output 2: Ramp w.t varying between 0 and 2*pi, synchronized on zero crossings of the fundamental (positive-sequence) of phase A. parameters are Minimum frequency (Hz):45, Initial inputs [Phase (degrees), Frequency (Hz)]:[0,60] and For optimal performance, set regulator gains [K_p K_i K_d] = [180 3200 1] and check the Enable Automatic Gain Control parameter. Com- pared to API, it has been found that the proposed controller results in more improvement of the DC-side volt-age within the operating frequency range of the ac-side of the ILC.

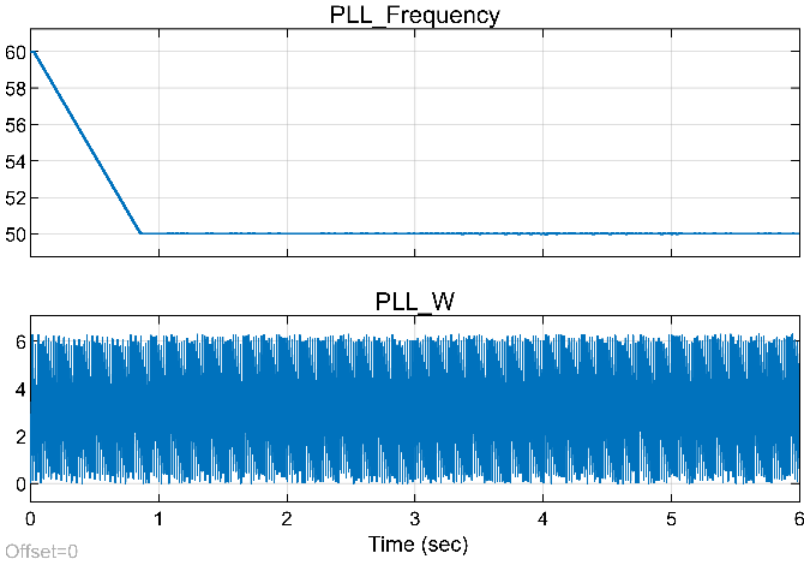

Fig.16. Response of PLL frequency and ω

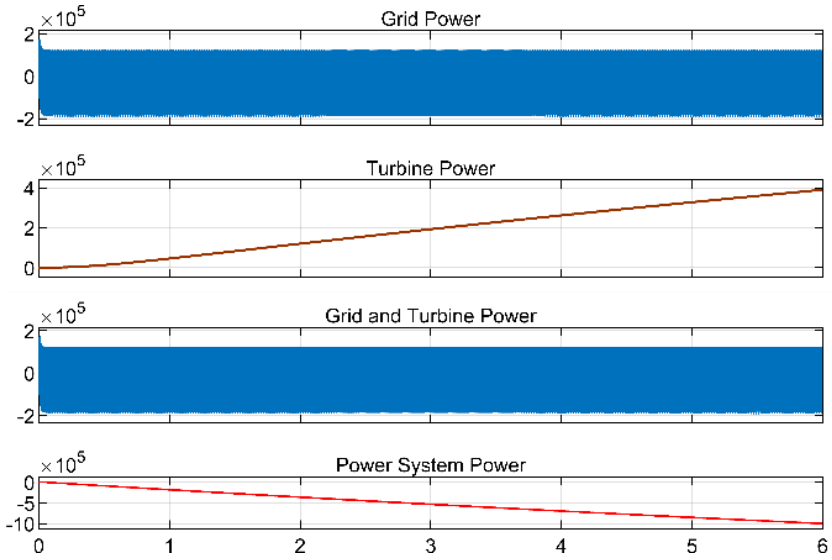

Fig.17.Response of Power for proposed powersystem powers

Fig. 17 appearances of grid, turbine, grid_turbine and finally power system outputs as present. Which has running 6 sec with different conditions however grid maintained constant output levels so turbine gives the residual power to the hybrid renewable energy sources. These results demonstrated the ability of the proposed redesigned interlinking converters to regulate power flow under all hybrid microgrid operating situations whilealso delivering the needed ancillary services. In the future, investigations on deep uncertainty analysis and stability analysis will be given, as well as the crea-tion of an intelligent control algorithm for the HMG.

Fig. 18 depicts the comparison graph for the overshoot voltage of converters. It shows the output voltage response with an overshoot of different converters' performance like P&O, FLC, and proposed converter. Based on the discussion the existing P&O method is unstable, and the FLC is stable but the proposed methodis more stable than these existing techniques. These perturbations are limited by the joint action of the output capacitor and the feedback control: the former limits the initial overshoot caused by a sudden change in load current, whereas the controller behaviour depends on the control circuit being used. From this Fig.18,

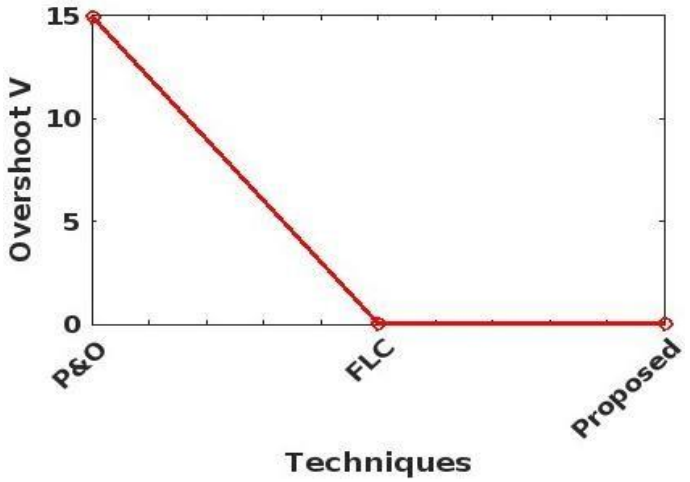

Fig.18. Comparison Graph for Overshoot Voltage

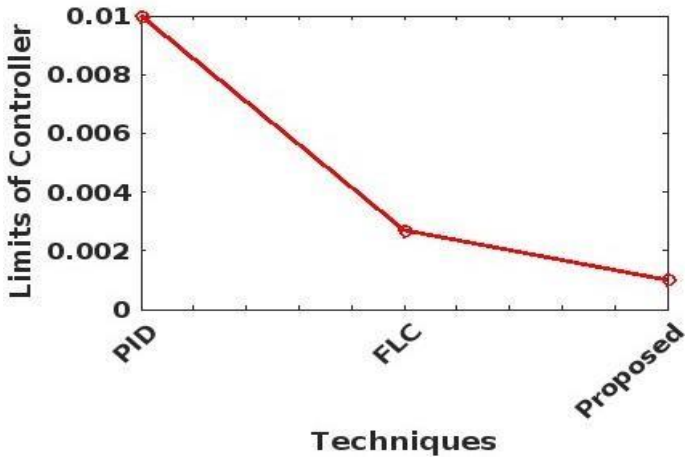

Fig.19. Comparison Graph for Limits of Controller

Fig. 19 depicts the comparison graph for Limits of Controller. In that The limits of the controller compared to the existing PID and FLC controllers are presented in this Fig. 19. The Fig. depicts that the limits of the PID controller are 0.01, and the limits of FLC controllers are 0.0027, however, the proposed method produces lower controller limits of 0.0013, respectively.

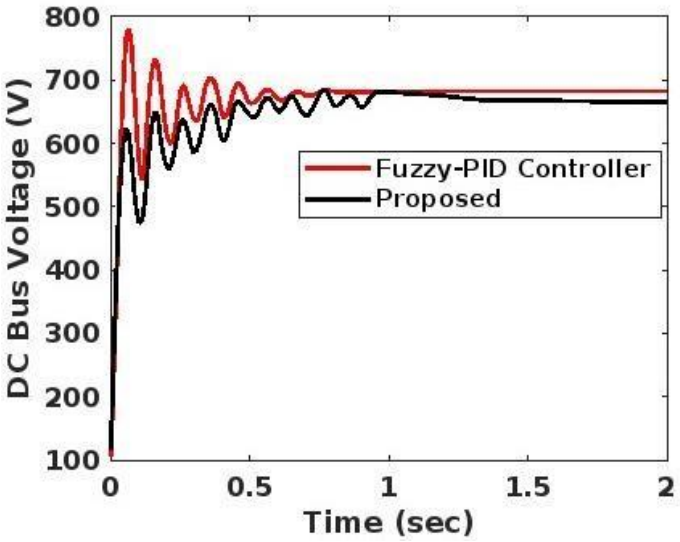

Fig.20 Comparison of DC Bus Voltage

Fig. 20 reveals the comparison graph for DC bus voltages, the proposed IT3-FLS controller is compared with the existing Fuzzy-PID controller. It can be observed that the error signal contains only the DC component due to the cancellation of the ripple component in the measured DC bus voltage. Consequently, the line currentwaveform is nearly sinusoidal.

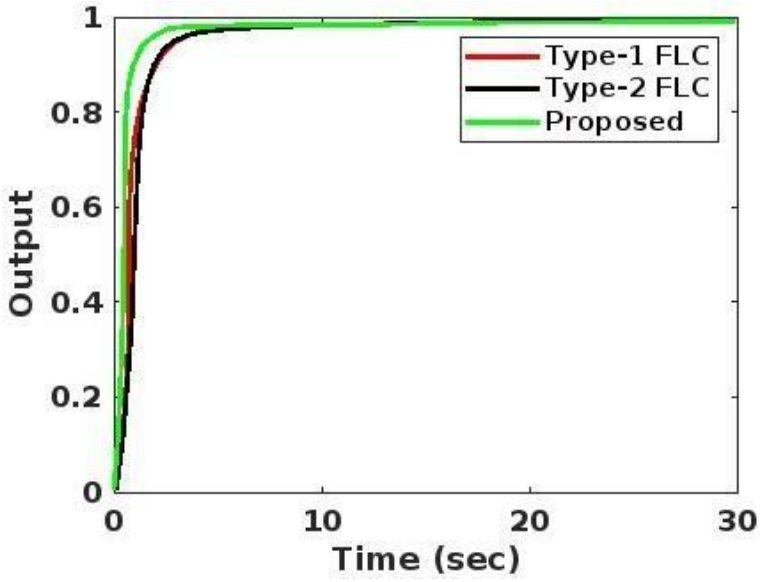

Fig.21. Comparison Graph for Dynamic Response of Controllers

Fig. 21 reveals the comparison graph of the dynamic response of different controllers. The proposed Interval Type-3 FLC is compared with the existing methods like Type-1 FLC, and Type-2 FLC. It evaluates the pro- posed method and knows the dynamic performance of the control system. From this Fig., the proposed method produces higher output dynamic response.

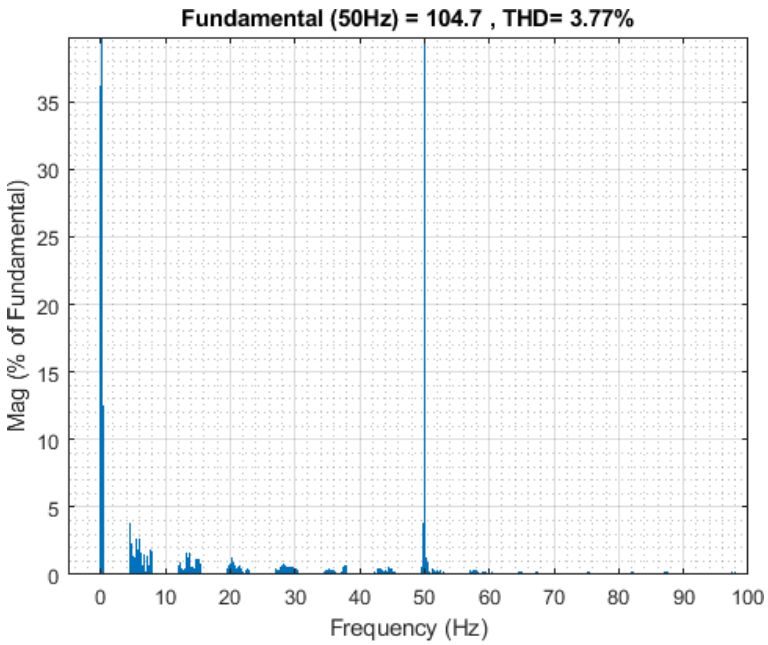

Fig.21. Grid Current % THD

From the IEEE – 519 Standard for Harmonic Control in Electric Power Systems suggests that total harmonicdistortion (THD) of the grid current has been maintained under 5% under all conditions. It is to be noted the grid current THD has been maintained under 3.77% as exposed in Fig. 21 and grid voltage THD has been maintained under 0.32% as presented in Fig. 22.

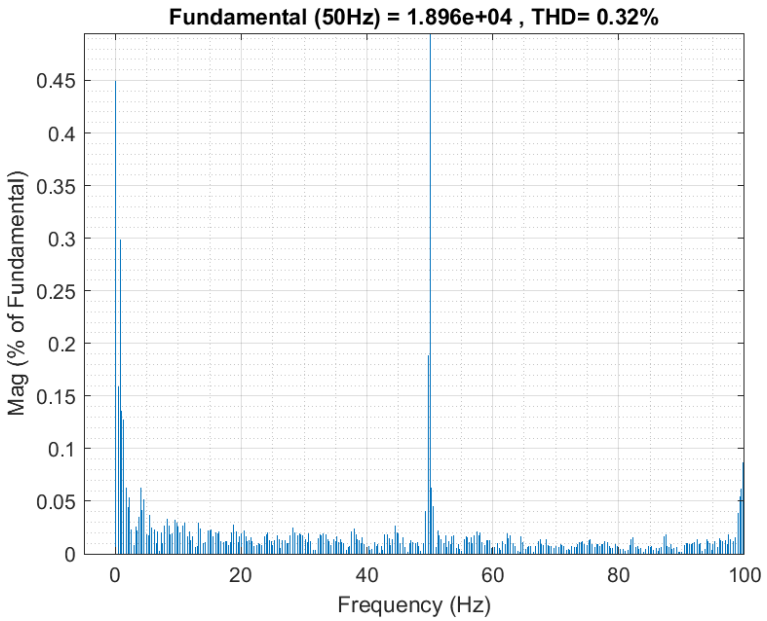

Fig.22. Grid Volatge % THD

Advanced hybrid AC/DC microgrid system integrating solar PV energy sources. A key feature of this systemis the AI-driven Maximum Power Point Tracking (MPPT) scheme used for the solar PV systems. In order to explore advanced control strategies, an interval type 3 fuzzy-based controller enhanced by the Bacterial For- aging Optimization Algorithm (BFOA) and interlinking drop control, ensure smooth operation and eliminationof harmonics. The grid voltage and current THD has been maintained under 5% with all conditions as per theIEEE-519 Standard.

5. Conclusion

A microgrid is a small-scale electrical system made up of distributed generation (DG) and energy storage devices (ESD) technologies designed to suit the needs of local loads. This paper proposes a Boost converter and a type-3 fuzzy controller, as well as a Swarm-based hybrid metaheuristic optimizer based on the Bacterial Foraging Optimization Algorithm (BFOA) for optimally tuning and managing the PI controller settings. Con- trolling the reactive power of the hybrid power system model using a Static Synchronous Compensator (STATCOM). In the MATLAB Simulink environment, a hybrid microgrid consisting of solar, battery, utilitygrid, and AC and DC loads is created using the AC and DC bus. The findings show that the suggested approach based on the algorithm outperforms the adaptive PI (API) controller in terms of rapid reaction time and tight regulation of power flow, voltage, and frequency under various situations. In comparison to API, the suggested controller improves the dc-side voltage within the working frequency range of the ac-side of the ILC. As a result, the penetration level characteristics are compared with the converter, and the suggested control approach is used to determine the efficiency of the hybrid power system. The grid voltage is 1.9 X 10^4 V, the battery current is around 1900 A for 6 seconds, and the voltage produced by the battery is around 190 V for 6 seconds. However, the acquired power-sharing diminishes the energy supplied by the power grid, avoiding focusing the required effort in the battery system. The power quality study demonstrated the efficiency of theinterlinking converters in reducing harmonic distortions and reactive power under all operating situations. Furthermore, the excellent performance of the voltage regulation, accomplished by a hierarchical control, was recorded and employed to rectify the voltage deviation induced by the droop technique. These results demonstrated the ability of the proposed redesigned interlinking converters to regulate power flow under all hybrid microgrid operating situations while also delivering the needed ancillary services. In the future, investigationson deep uncertainty analysis and stability analysis will be given, as well as the creation of an intelligent controlalgorithm for the HMG.

References

[1] Mehta, S., & Basak, P. (2021, February 17). A comprehensive review on control techniques for stability improvement in microgrids. https://doi.org/10.1002/2050-7038.12822

[2] Rajan, C S., & Ebenezer, M. (2020, December 17). Modeling Operation and Simulation of Interconnected DC Microgrids. https://doi.org/10.1109/picc51425.2020.9362454

[3] Safder, M U., Sanjari, M J., Hamza, A., Garmabdari, R., Ma, H., & Lu, J. (2023, September 5). Enhancing Microgrid Stability and Energy Management: Techniques, Challenges, and Future Directions. https://doi.org/10.3390/en16186417

[4] Wang, H., Li, W., Yue, Y., & Zhao, H. (2021, December 22). Distributed Economic Control for AC/DC Hybrid Microgrid. https://doi.org/10.3390/electronics11010013

[5] S. Bhattacharyya, D. S. K. Patnam, S. Samanta et al., "Steady outputand fast tracking MPPT (SOFT MPPT) for P&O and InC algorithm," IEEE Transactions on Sustainable Energy. doi: 10.1109/TSTE. 2020.2991768

[6] Y. Yang and H. Wen, "Adaptive perturb and observe maximum power point tracking with current predictive and decoupled power control for grid connected photovoltaic inverters," Journal of Modern Power Systems and Clean Energy, vol. 7, no. 2, pp. 422-432, Mar. 2019

[7] Gamil, M.M., Senjyu, T., Masrur, H., Takahashi, H. and Lotfy, M.E., 2022. Controlled V2Gs and battery integration into residential microgrids: Economic and environmental impacts. Energy Conversion and Management, 253, p.115171.

[8] Gui, Y., Han, R., Guerrero, J.M., Vasquez, J.C., Wei, B. and Kim, W., 2021. Large-Signal stability improvement of DC-DC converters in DC microgrid. IEEE Transactions on Energy Conversion, 36(3), pp.2534-2544.

[9] Jabeur, R., Boujoudar, Y., Azeroual, M., Aljarbouh, A. and Ouaaline, N., 2022. Microgrid energy management system for smart home using multi-agent system. International Journal of Electrical & Computer Engineering (2088-8708), 12(2).

[10] Al Sumarmad, K.A., Sulaiman, N., Wahab, N.I.A. and Hizam, H., 2022. Energy Management and Voltage Control in Microgrids Using Artificial Neural Networks, PID, and Fuzzy Logic Controllers. Energies, 15(1), p.303.

[11] Ali, A., & Majhi, S. (2006, January 1). Design of Optimum PID Controller by Bacterial Foraging Strategy. https://doi.org/10.1109/icit.2006.372205

[12] Jhankal, N K., & Adhyaru, D M. (2011, December 1). Bacterial foraging optimization algorithm: A derivative free technique. https://doi.org/10.1109/nuicone.2011.6153240

[13] Yarima, S M., Jiya, J D., & Buhari, M D. (2016, October 1). A bacterial foraging algorithm optimized fuzzy logic for power control of code division multiple access cellular systems. https://doi.org/10.1109/icsae.2016.7810153

[14] Punna, S., Mailugundla, R. and Salkuti, S.R., 2022. Design, Analysis and Implementation of Bidirectional DC–DC Converters for HESS in DC Microgrid Applications. Smart Cities, 5(2), pp.433-454.

[15] Vinothkumar, J., & Thamizhselvan, R. (2023). Enhancing controller efficiency in hybrid power system using interval type 3 fuzzy controller with bacterial foraging optimization algorithm. J. Theor. Appl. Inf. Technol, 101, 12

[16] Ahmed, M., Magdy, G., Khamies, M. and Kamel, S., 2022. An efficient coordinated strategy for frequency stability in hybrid power systems with renewables considering interline power flow controller and redox flow battery. Journal of Energy Storage, 52, p.104835.

[17] Dei, G., Gupta, D.K., Sahu, B.K., Jha, A.V., Appasani, B., Zawbaa, H.M. and Kamel, S., 2022. Improved Squirrel Search Algorithm Driven Cascaded 2DOF-PID-FOI Controller for Load Frequency Control of Renewable Energy Based Hybrid Power System. IEEE Access, 10, pp.46372-46391.

[18] Kumar, A., Gupta, D.K. and Ghatak, S.R., 2022, January. Fractional order PI Controller based Load Frequency Control of Hybrid Power System with Electric Vehicle. In 2022 2nd International Conference on Power Electronics & IoT Applications in Renewable Energy and its Control (PARC) (pp. 1-6). IEEE.

[19] Sharma, M., Saxena, S., Prakash, S., Dhundhara, S. and Arya, Y., 2022. Frequency stabilization in sustainable energy sources integrated power systems using novel cascade noninteger fuzzy controller. Energy Sources, Part A: Recovery, Utilization, and Environmental Effects, 44(3), pp.6213-6235.

[20] Eluri, H. and Naik, M.G., 2022. Energy Management System and Enhancement of Power Quality with Grid Integrated Micro-Grid using Fuzzy Logic Controller. IJEER, 10(2), pp.256-263.

[21] Sundararaju, N., Vinayagam, A., Veerasamy, V. and Subramaniam, G., 2022. A Chaotic Search-Based Hybrid Optimization Technique for Automatic Load Frequency Control of a Renewable Energy Integrated Power Sys- tem. Sustainability, 14(9), p.5668.

[22] Kumar, A. and Suhag, S., 2022. Whale optimization algorithm optimized fuzzy-pid plus pid hybrid controller for frequency regulation in hybrid power system. Journal of The Institution of Engineers (India): Series B, 103(2), pp.633-648.

[23] Aryan Nezhad, M., 2022. Frequency Control and Power Balancing in a Hybrid Renewable Energy System (HRES): Effective Tuning of PI Controllers in the Secondary Control Level. Journal of Solar Energy Research, 7(1), pp.963-970.

[24] Zhang, Y., Cheng, C., Cai, H., Jin, X., Jia, Z., Wu, X., Su, H. and Yang, T., 2022. Long-term stochastic model predictive control and efficiency assessment for hydro-wind-solar renewable energy supply system. Applied En- ergy, 316, p.119134.
[25] Chitra, L. and Kavitha Kumari, K.S., 2022. Artificial Intelligent Based Control of Improved Converter for Hybrid Renewable Energy Systems. In Proceedings of International Joint Conference on Advances in Computational Intel- ligence (pp. 583-596). Springer, Singapore.
[26] Hu, J., Jin, N., Li, P., & Zhang, H. (2020, September 1). An Improved Bacterial Foraging Algorithm for Multi-modal Problems. IOP Publishing, 1631(1), 012069-012069. https://doi.org/10.1088/1742-6596/1631/1/012069
[27] Mai, X., & Li, L. (2016, August 1). An enhanced bacterial foraging optimization with adaptive elimination-dispersal probability and PSO strategy. https://doi.org/10.1109/fskd.2016.7603168
[28] Yarima, S M., Jiya, J D., & Buhari, M D. (2016, October 1). A bacterial foraging algorithm optimized fuzzy logic for power control of code division multiple access cellular systems. https://doi.org/10.1109/icsae.2016.7810153
[29] Liu, L., Zhou, W., Guan, K., Peng, B., Xu, S., Tang, J., Zhu, Q., Till, J L., Jia, X., Jiang, C., Wang, S., Qin, Z., Kong, H., Grant, R F., Mezbahuddin, S., Kumar, V., & Jin, Z. (2024, January 8). Knowledge-guided machine learning can improve carbon cycle quantification in agroecosystems. https://doi.org/10.1038/s41467-023-43860-5
[30] Gusmão, G S., Retnanto, A P., Cunha, S C D., & Medford, A J. (2023, May 1). Kinetics-informed neural networks. https://doi.org/10.1016/j.cattod.2022.04.002
[31] Wang, P., Li, M., Zhou, C., Hu, Z., & Yin, H. (2018, December 1). Numerical simulations of flow and mass transfer during large-scale potassium dihydrogen phosphate crystal growth via three-dimensional motion growth method. Elsevier BV, 127, 901-907. https://doi.org/10.1016/j.ijheatmasstransfer.2018.08.098
[32] J. J. Khanam and S. Y. Foo, "Modeling of a photovoltaic array in MATLAB Simulink and maximum power point tracking using neural network," Electrical & Electronic Technology Open Access Journal, vol. 2, no. 2, pp. 40-46, Jul. 2018.
[33] L. Chen and X. Wang, "An enhanced MPPT Method based on ANN- assisted sequential Monte Carlo and quickest change detection," IET Smart Grid, vol. 2, no. 4, pp. 635-644, Dec. 2019.
[34] Rickard, J.T.; Aisbett, J.; Gibbon, G. Fuzzy Subsethood for Fuzzy Sets of Type-2 and Generalized Type-n. IEEE Trans. Fuzzy Syst.2008, 17, 50–60. [CrossRef]
[35] Mohammadzadeh, A.; Sabzalian, M.H.; Zhang, W. An Interval Type-3 Fuzzy System and a New Online Fractional-Order Learning Algorithm: Theory and Practice. IEEE Trans. Fuzzy Syst. 2019, 28, 1940–1950. [CrossRef]
[36] Liu, Z.; Mohammadzadeh, A.; Turabieh, H.; Mafarja, M.; Band, S.S.; Mosavi, A. A New Online Learned Interval Type-3 FuzzyControl System for Solar Energy Management Systems. IEEE Access 2021, 9, 10498–10508. [Cross-Ref]
[37] Castillo, O.; Castro, J.R.; Melin, P. Interval Type-3 Fuzzy Systems: Theory and Design; Springer: Berlin/Heidelberg, Germany, 2022.[CrossRef]

AUTHOR BIOGRAPHIES

Mr.D VenkataBramhanaidu was born in Andhra- Pradesh, India. He received his B.Tech degree in Electrical and Electronics Engineering from JNTU Hyderabad, Telangana, India in 2010. He received his M.Tech degree in Power Electronics and Electrical Drives from JNTU Hyderabad, Telangana in 2014. He is currently pursuing Ph.D in Electrical Engg, Annamalai University and working in S.V.U College of Engineering, S.V.University, Tirupati, AP, India. His areas of interests are Microgrid, Renewable Energy Sources Power Electronics, Electrical drives and the application of Soft Computing techniques. He has published his works in various international and national journals. Having Life Memberships of ISCA, IE(India), ISTE,IAENG and IFERP.

Dr. R. Thamizhselvan serves as an Associate Professor of Electrical Engineering at Annamalai University, located in Tamil Nadu, India. He earned his Bachelor's degree in Electrical and Electronics Engineering from Annamalai University in 2004, followed by a Master of Engineering in Power Systems in 2008, also from Annamalai University. He furthered his academic pursuits by completing his Ph.D. in Electrical Engineering in 2017.Currently, he is on assignment at Government Technical Institutions under the Directorate of Technical Education in Chennai. His research focuses including Power System Security, Renewable Energy, Microgrid, and the application of Soft Computing techniques in Power Systems. He is a lifetime member of IOE(India), ISTE&IAENG

.

Dr. Ch. Chengaiah, Professor in Sri Venkateswara University, Tirupati, Andhra Pradesh. He received his B.Tech degree in Electrical and Electronics Engineering from S.V.U College of Engineering, Tirupati, AP in 1999. He received his M.E degree in Power Systems from National Institute of Technology formerly called as REC, Tiruchirapalli, TN in 2000 and He received his Ph.D. degree in Power Systems Operation and Control from Sri Venkateswara University in 2013. With 21 years of teaching experience under his girdle, he has successfully concluded three funded research projects. His research interests include Power System and Control Engineering, Renewable Energy Systems, Power Electronics and Drives.